The Constrained NMSSM with a 126 GeV Higgs boson – A global analysis

Kamila Kowalska, Shoaib Munir, Leszek Roszkowski*, Enrico Maria Sessolo, Sebastian Trojanowski, Yue-Lin Sming Tsai

BayesFITS Group
National Centre for Nuclear Research, Hoża 69, 00-681 Warsaw, Poland

Kamila.Kowalska@fuw.edu.pl, Shoaib.Munir@fuw.edu.pl,
L.Roszkowski@sheffield.ac.uk, Enrico-Maria.Sessolo@fuw.edu.pl,
Sebastian.Trojanowski@fuw.edu.pl, Sming.Tsai@fuw.edu.pl

December 11, 2012

Abstract

We present the first global analysis of the Constrained NMSSM that investigates the impact of the recent discovery of a 126 GeV Higgs-like boson, of the observation of a signal for $\mathrm{BR}(\mathrm{B_s} \to \mu^+\mu^-)$, and of constraints on supersymmetry from $\sim 5/\mathrm{fb}$ of data accumulated at the LHC, as well as of other relevant constraints from colliders, flavor physics and dark matter. We consider three possible cases, assuming in turn that the discovered Higgs boson is: i) the lightest Higgs boson of the model; ii) the next-to-lightest Higgs boson; and iii) a combination of both roughly degenerate in mass. The likelihood function for the Higgs signal uses signal rates in the $\gamma\gamma$ and $ZZ \to 4l$ channels, while that for the Higgs exclusion limits assumes decay through the $\gamma\gamma$, $\tau\tau$, ZZ and W^+W^- channels. In all cases considered we identify the 68% and 95% credible posterior probability regions in a Bayesian approach. We find that, when the constraints are applied with their respective uncertainties, the first case shows strong CMSSM-like behavior, with the stau coannihilation region featuring highest posterior probability, the best-fit point, a correct mass of the lightest Higgs boson and the lighter stop mass in the ballpark of 1 TeV. We also expose in this region a linear relationship between the trilinear couplings of the stau and the stop, with both of them being strongly negative as enforced by the Higgs mass and the relic density, which outside of the stau coannihilation region show some tension. The second and the third case, on the other hand, while allowed are disfavored by the constraints from direct detection of dark matter and from $\mathrm{BR}(\mathrm{B_s} \to \mu^+\mu^-)$. Without the anomalous magnetic moment of the muon the fit improves considerably, especially for negative effective μ parameter. We discuss how the considered scenarios could be tested furtherly at the LHC and in dark matter searches.

*On leave of absence from the University of Sheffield, UK.

1 Introduction

In July 2012 the CMS and ATLAS collaborations at the LHC made the announcement of a $\sim 5\sigma$ discovery of a boson with mass $125.3 \pm 0.6\,\text{GeV}$ [1] and $126.0 \pm 0.6\,\text{GeV}$ [2], respectively, consistent with the Higgs boson predicted by the electroweak (EW) Standard Model (SM). The CMS Collaboration has recently updated its results [3] to $125.8 \pm 0.6\,\text{GeV}$. The updated result is based on the analysis of the data corresponding to integrated luminosities of 5.1/fb at $\sqrt{s} = 7\,\text{TeV}$ and up to 12.2/fb at $\sqrt{s} = 8\,\text{TeV}$ in the $\gamma\gamma$, ZZ, WW, $\tau\tau$ and bb decay channels. The ATLAS analysis combined approximately 4.8/fb of 2011 data at $\sqrt{s} = 7\,\text{TeV}$ in the same five channels with 5.8/fb of data at $\sqrt{s} = 8\,\text{TeV}$ in the ZZ, $\gamma\gamma$ and WW channels only. Evidently, the excess of events near the reported mass is driven by the $\gamma\gamma$ and ZZ channels, owing to the highest mass resolution of these channels. Both collaborations also determined the ratio $\mu(X)$ of the observed Higgs production cross section to the one predicted by the SM, in each of the mentioned Higgs decay channels X. An enhancement in the $\gamma\gamma$ channel was reported by ATLAS, with $\mu(\gamma\gamma) = 1.9 \pm 0.5$, as well as by CMS, with $\mu(\gamma\gamma) = 1.6 \pm 0.4$. On the other hand, the updated value of $\mu(ZZ)$ by CMS [4] and ATLAS [5] is, within 1σ error, SM-like.

While its exact characteristics are still being carefully examined, such a boson is not only consistent with the SM Higgs particle but can also be easily accommodated into models of new physics, particularly those based on softly-broken low-energy supersymmetry (SUSY) which actually predict a relatively light Higgs boson. Most studies have been performed within the framework of the two Higgs doublet Minimal Supersymmetric Standard Model (MSSM), usually augmented by various unification boundary conditions. The framework, however, suffers from the so-called 'μ-problem' [6]: the SUSY-preserving parameter μ in the superpotential is expected to be of the order of the SUSY breaking scale $M_{\text{SUSY}} \sim 1\,\text{TeV}$ to assure correct radiative EW symmetry breaking.

Perhaps the most compelling and simplest solution to the μ-problem is to invoke an additional gauge singlet field coupled to the Higgs doublets of the MSSM [6]. The μ-term is then generated dynamically through the vacuum expectation value (vev) of the singlet field which is of the order of M_{SUSY}. The model is commonly referred to as the Next-to-Minimal Supersymmetric Standard Model (NMSSM); for reviews see, e.g., [7, 8]. After the discovery of the Higgs-like boson, numerous studies have appeared in the context of the NMSSM [9, 10, 11, 12, 13], since the model presents several interesting features. In the NMSSM the particle content remains the same as in the MSSM, except that the number of Higgs bosons increases from three to five: three neutral scalars $h_{1,2,3}$ and two neutral pseudoscalars $a_{1,2}$. The number of neutralinos also increases from four to five, $\chi_{1,\ldots,5}$, owing to the singlino partner of the singlet Higgs boson.

On the phenomenological front, a two-loop theoretical upper bound on the mass of the lightest CP-even Higgs boson, m_{h_1}, can increase by a few GeV compared to the MSSM for some combinations of the model's parameters. Moreover, in the context of the recent LHC results, the next-to-lightest CP-even Higgs boson of the model, h_2, could also have mass around 126 GeV with h_1 being even lighter than the LEP bound on SM-like Higgs boson mass, without violating it [14, 15], owing to the singlet-doublet mixing effects. Both features potentially allow to achieve the correct mass of the experimentally detected Higgs without excessive fine-tuning [16, 17, 18, 19], making the NMSSM potentially a more 'natural' model than the MSSM. Finally, the NMSSM also offers the additional possibility that the observed excess in the $\gamma\gamma$ and ZZ rates could be due to the combination of h_1 and h_2 decays (with m_{h_1} and m_{h_2} being almost degenerate) [10]. Besides masses, the decay rates of the Higgs boson(s) are also affected by the modifications in the superpotential. For example, for large doublet-singlet mixing, the $h_1 b\bar{b}$ coupling becomes suppressed, reducing the total decay width. As a result, the branching ratio (BR) of $h_1 \to \gamma\gamma$ becomes marginally enhanced compared to the SM or the MSSM [20]. An important consequence of this feature is that h_1 lighter

than 115 GeV could have escaped detection at LEP, and also at the LHC, due to the possibility of its decay into a pair of the two lighter pseudoscalars, $h_1 \to a_1 a_1$ (see, e.g., [21]), causing thus a suppression in all of the other BR's of h_1.

The NMSSM in its most general form contains more than a hundred free parameters: those appearing in the MSSM and some additional ones relating to the extended Higgs sector. Similarly to the MSSM, where imposing universality conditions on the soft SUSY-breaking parameters of the model at the scale of grand unification (GUT scale) leads to the Constrained MSSM (CMSSM) [22], a GUT-constrained version of the NMSSM (CNMSSM) [23, 24, 25] can be defined; see Sec. 2 for more details and discussion.

It is well known that, in the CMSSM the lightest Higgs boson's mass, as calculated at 2-loop level with FeynHiggs [26] or SoftSusy [27], is typically a few GeV below 126 GeV, which can be considered as somewhat unsatisfactory even if one takes into account a residual error of some 2–3 GeV [28] from scheme dependence. (Values of m_h around 126 GeV can still be obtained in the CMSSM for $M_{\rm SUSY} \gg 1$ TeV at the expense of increased fine-tuning [29].) A priori one could expect that in the CNMSSM, with more freedom in the Higgs sector, the tension will be reduced. However, recent studies [30] using a fixed-grid scan approach have shown that in the CNMSSM it is extremely difficult to obtain a Higgs boson as heavy as 126 GeV, particularly one with an enhanced $\gamma\gamma$ decay rate, while also satisfying other phenomenological constraints, thus nullifying the noted advantages of the singlet-extension of the MSSM.

On the other hand, it has been demonstrated by our recent global analysis of the CMSSM [29] and by some earlier Bayesian studies [31, 32], that a proper treatment of the experimental constraints through a likelihood function can lead to significantly different results from fixed-grid scans where such constraints are typically implemented in a more simplified box-like fashion, with all points accepted when satisfying experimental values within some fixed range (typically within 1σ, or so), and otherwise rejected. One of the main advantages of the statistical approach is that scanned points are instead 'weighted' by the total χ^2, thus indicating how well they fit all constraints. For example, in the fixed-grid approach a point giving a value of even one constraint slightly beyond the allowed range while reproducing central values of all the other constraints would be rejected, while a point with values for all the constraints barely within the allowed boxes would be completely allowed. In contrast, in a statistical approach both points would be accepted but weighted with their respected χ^2. Another advantage of the statistical approach based on the likelihood function is that theoretical and experimental uncertainties can be easily implemented in a consistent manner. Thanks to some recent developments in sampling algorithms (see, e.g., [33] and [34]), multidimensional Bayesian scans can now be carried out rather quickly and efficiently.

One should note two important changes in the data that have recently taken place on the experimental front. In November 2012 the LHCb Collaboration published the most recent update of their search for the rare decay $B_s \to \mu^+\mu^-$ [35], reporting an excess of $B_s \to \mu^+\mu^-$ candidates over the background. The measured value, $\mathrm{BR}\,(\mathrm{B_s} \to \mu^+\mu^-) = 3.2^{+1.5}_{-1.2} \times 10^{-9}$, is now very close to the time-averaged SM value, 3.5×10^{-9} [36, 37]. We include the constraint in our likelihood function taking into account both theoretical and experimental uncertainties, as will be described below.

The other important update was the top pole mass by the Particle Data Group, obtained from an average of data from Tevatron and the LHC at $\sqrt{s} = 7$ TeV, $M_t = 173.5 \pm 1.0$ GeV [38]. As we shall see below this is a welcome increase relative to its previous value in the context of the Higgs sector of constrained SUSY models as it pushes the mass of h_1 up, closer to the experimentally observed Higgs-like resonance mass.

In this article, we present the first global Bayesian analysis of the CNMSSM after the observation of the SM Higgs-like boson. We separately consider the cases of this boson being h_1, or h_2, or a

combination of both. We test the parameter space of the model against the currently published, already stringent constraints from SUSY searches at the LHC and other relevant constraints from colliders, b-physics and dark matter (DM) relic density. Our goal is to map out the regions of the parameter space of the CNMSSM that are favoured by these constraints. As in our CMSSM study [29], the CMS razor limit based on 4.4/fb of data is implemented through an approximate but accurate likelihood function. We also study the effects of relaxing the $(g-2)_\mu$ constraint.

The article is organized as follows. In Sec. 2 we briefly revisit the model, highlighting some of its salient features. In Sec. 3 we detail our methodology, including our statistical approach and our construction of the likelihoods for the BR$(\mathrm{B_s} \to \mu^+\mu^-)$ signal, the CMS razor 4.4/fb analysis, and the CMS Higgs searches. In Sec. 4 we present the results from our scans and discuss their novel features. We summarize our findings in Sec. 5.

2 The NMSSM with GUT-scale universality

The NMSSM is an economical extension of the MSSM, in which one adds a gauge-singlet superfield S whose scalar component couples only to the two MSSM Higgs doublets H_u and H_d at the tree-level.[1] The scale-invariant superpotential of the model has the form

$$W = \lambda S H_u H_d + \frac{\kappa}{3} S^3 + (\text{MSSM Yukawa terms}) \,, \tag{1}$$

where λ and κ are dimensionless couplings. Upon spontaneous symmetry breaking, the scalar Higgs field S develops a vev, $s \equiv \langle S \rangle$, and the first term in Eq. (1) assumes the role of the effective μ-term of the MSSM, $\mu_{\rm eff} = \lambda s$. The soft SUSY-breaking terms in the Higgs sector are then given by

$$V_{\rm soft} = m_{H_u}^2 |H_u|^2 + m_{H_d}^2 |H_d|^2 + m_S^2 |S|^2 + \left(\lambda A_\lambda S H_u H_d + \frac{1}{3} \kappa A_\kappa S^3 + \text{h.c.} \right) \,, \tag{2}$$

where A_λ and A_κ are soft trilinear terms associated with the λ and κ terms in the superpotential. The vev s, determined by the minimization conditions of the Higgs potential, is effectively induced by the SUSY-breaking terms in Eq. (2), and is naturally set by $M_{\rm SUSY}$, thus solving the μ-problem of the MSSM.

The Constrained version of the NMSSM (CNMSSM) is defined in terms of five continuous input parameters and one sign,

$$m_0, m_{1/2}, A_0, \tan\beta, \lambda, \mathrm{sgn}(\mu_{\rm eff}) \,, \tag{3}$$

where unification conditions at a high scale require that all the scalar soft SUSY-breaking masses in the superpotential (except m_S) are unified to m_0, the gaugino masses are unified to $m_{1/2}$, and all trilinear couplings, including A_λ and A_κ, are unified to A_0. Additionally, $\tan\beta$ (the ratio of the vevs of the neutral components of the H_u and H_d fields) and $\mathrm{sgn}(\mu_{\rm eff})$ are taken as input at the weak scale, and λ is an input parameter at $M_{\rm SUSY}$. The singlet soft-breaking mass m_S^2 is not unified to m_0^2 for both theoretical and phenomenological reasons. From the theoretical point of view, it has been argued [39] that the mechanism for SUSY breaking might treat the singlet field differently from the other superfields. From the phenomenological point of view, the freedom in m_S allows for easier convergence when the renormalization group equations (RGE's) are evolved from the GUT scale down to $M_{\rm SUSY}$. It also yields, in the limit $\lambda \to 0$, and with λs fixed, effectively the CMSSM plus a singlet and singlino fields that both decouple from the rest of the spectrum.

[1] For simplicity we will be using the same notation for superfields and their bosonic components.

Measurement	Mean or Range	Error: (Exp., Th.)	Distribution	Ref.
CMS razor 4.4/fb	See text	See text	Poisson	[42]
$m_{h_{\rm sig}}$	125.8 GeV	0.6 GeV, 3 GeV	Gaussian	[3]
$R_{h_{\rm sig}}(\gamma\gamma)$	1.6	0.4, 15%	Gaussian	[1]
$R_{h_{\rm sig}}(ZZ)$	0.80	$+0.35-0.28$, 15%	Gaussian	[4]
$m_{h_{\rm hid}}$ (GeV)	< 122.7 GeV, > 128.9 GeV	0, 3 GeV	Error Fn	See text
$R_{h_{\rm hid}}(\gamma\gamma, ZZ, \tau\tau, WW)$	See text	0, 15%	Error Fn	[43]
$\Omega_\chi h^2$	0.1120	0.0056, 10%	Gaussian	[44]
$\delta\,(g-2)_\mu^{\rm SUSY}\times 10^{10}$	28.7	8.0, 1.0	Gaussian	[38, 45]
BR $(\overline{\rm B}\to {\rm X_s}\gamma)\times 10^4$	3.43	0.22, 0.21	Gaussian	[46]
BR $({\rm B_u}\to\tau\nu)\times 10^4$	1.66	0.66, 0.38	Gaussian	[47]
ΔM_{B_s}	17.719 ps^{-1}	0.043 ps^{-1}, 2.400 ps^{-1}	Gaussian	[38]
BR $({\rm B_s}\to\mu^+\mu^-)$	3.2×10^{-9}	$+1.5-1.2$, 10%	Gaussian	[35]

Table 1: The experimental constraints that we apply to constrain model parameters. $m_{h_{\rm sig}}$, $m_{h_{\rm hid}}$, $R_{h_{\rm sig}}$ and $R_{h_{\rm hid}}$ are defined in Sec. 3.3.

3 Statistical treatment of experimental data

We explore the parameter space of the model with the help of Bayesian formalism. We follow the procedure outlined in detail in our previous papers [40, 41, 29], of which we give a short summary here. Our aim is to map out the 68% and 95% credible regions of $p(m|d)$, the posterior probability density function (pdf), given by Bayes' theorem,

$$p(m|d) = \frac{p(d|\xi(m))\pi(m)}{p(d)}\,. \tag{4}$$

$p(d|\xi(m)) \equiv \mathcal{L}$ is the likelihood function, which describes the probability of obtaining the data d given the computed value of some observable $\xi(m)$, which is a function of the model's parameters m. $\mathcal{L}$ also incorporates the experimental and theoretical uncertainties. Prior probability $\pi(m)$ encodes assumed range and distribution of m. Finally, $p(d)$ is the evidence, which is a normalization constant as long as only one model is considered, but serves as a comparative measure for different models or scenarios.

Bayes' theorem provides an efficient and natural procedure for drawing inferences on a subset of r specific model parameters (including nuisance parameters), or observables, or a combination of both, which we collectively denote by ψ_i. They can be obtained through marginalization of the full posterior pdf, carried out as

$$p(\psi_{i=1,..,r}|d) = \int p(m|d)d^{n-r}m\,, \tag{5}$$

where n is the total number of input parameters. An analogous procedure can be performed with the observables and with a combination of the model's parameters and observables.

In order to evaluate the posterior probability given by Eq. (4), one needs to first construct the likelihood function. The constraints that we include in the current analysis are listed in Table 1. We shall be discussing them in turn below. As a rule, following the procedure developed earlier [48], we implement positive measurements through the usual Gaussian likelihood, while upper or lower limits through an error function smeared with both theory and, when available, experimental error. The construction of the likelihoods for direct SUSY and Higgs searches is more involved, and will be explained in detail later in this section.

3.1 Likelihood for $\mathrm{BR}(\mathrm{B_s} \to \mu^+\mu^-)$

In November 2012 the LHCb Collaboration published the most recent update of their search for the rare decay $B_s \to \mu^+\mu^-$ [35], based on a combination of the 2012 data samples of 1.1/fb of proton-proton collisions at $\sqrt{s} = 8\,\mathrm{TeV}$ and the 2011, 1.0/fb data at $\sqrt{s} = 7\,\mathrm{TeV}$. The data superseded the combination of 2011 data from ATLAS, CMS and LHCb published in June 2012 [49].

LHCb observed an excess of $B_s \to \mu^+\mu^-$ candidates over the background, consistent with the SM expectation. The measured value is $\mathrm{BR}(\mathrm{B_s} \to \mu^+\mu^-) = 3.2^{+1.5}_{-1.2} \times 10^{-9}$, with a statistical significance of $3.5\,\sigma$. We used this information to construct an approximate likelihood function for $\mathrm{BR}(\mathrm{B_s} \to \mu^+\mu^-)$ which parametrizes the experimental and theoretical uncertainties. The most important sources of theoretical uncertainty are the B_s decay constant (main contribution) and its lifetime, the top quark mass and the CKM matrix elements $V_{tb}^* V_{ts}$ [37] and their total amounts to approximately 11% of the mean value [50]. Thus, we parametrized the likelihood function as a combination of two half-Gaussians, to take into account the asymmetry in the experimental uncertainty. A theoretical uncertainty equal to 10% of the calculated value was added in quadrature. Notice that we neglected the uncertainty due to the top pole mass ($\sim 1\%$) since it is taken care of by scanning over the SM nuisance parameters (see below).

3.2 Limits on SUSY from the LHC

In Ref. [29] we derived a methodology for constructing an approximate likelihood map that reproduced the lower limit in the (m_0, $m_{1/2}$) plane set by the CMS Collaboration by applying the razor method [51, 42] to SUSY searches in all-hadronic modes based on 4.4/fb of data. We validated our map against the experimental results by evaluating the resulting 95% CL contour in the (m_0, $m_{1/2}$) plane and comparing it with the corresponding 95% CL exclusion limit provided by the CMS Collaboration. We obtained a very good agreement confirming that our procedure for generating these likelihood maps was indeed correct. Our methodology can be applied to produce the SUSY exclusion limits in any R-parity conserving supersymmetric model, as long as the supersymmetric spectra in that model present similar features to the ones of the CMSSM, namely a sufficient mass difference between the lightest SUSY particle (LSP) and gluinos or squarks of the first two generations. When extending the procedure to other models, one should also take into account possible changes in the production and decay modes of the particles. In this paper we follow the same methodology for generating a SUSY likelihood map based on the CMS razor 4.4/fb analysis for the NMSSM.

For each point in an $m_0 - m_{1/2}$ grid, with 50 GeV step size in both parameters, the supersymmetric mass spectrum and decay table are generated using NMSSMTools [52], and fed into Herwig++ [53] for parton shower generation and calculation of the cross sections. Herwig++ allows one to work in the framework of the NMSSM, and hence takes care of a possible contribution from the extended neutralino and Higgs sectors. The production modes are not influenced by these sectors, since the razor search is designed to detect squarks and gluinos, which are produced through color interactions. The output of Herwig++ is passed in HepMC [54] format to Delphes [55] for reconstruction of the physical objects by simulating the CMS detector's response. The output from Delphes is distributed into 38 bins, defined in terms of the razor variables M_R and R^2, each containing the data (a number of background and signal events) from the experiment, to produce an efficiency map for each bin, which is then translated into a likelihood map for the whole grid. We refer the reader to Ref. [29] for more details of the complete procedure adopted for the production of efficiency maps.

The 95% CL razor contour thus reproduced is shown in Fig. 1. The actual 95% CL line obtained

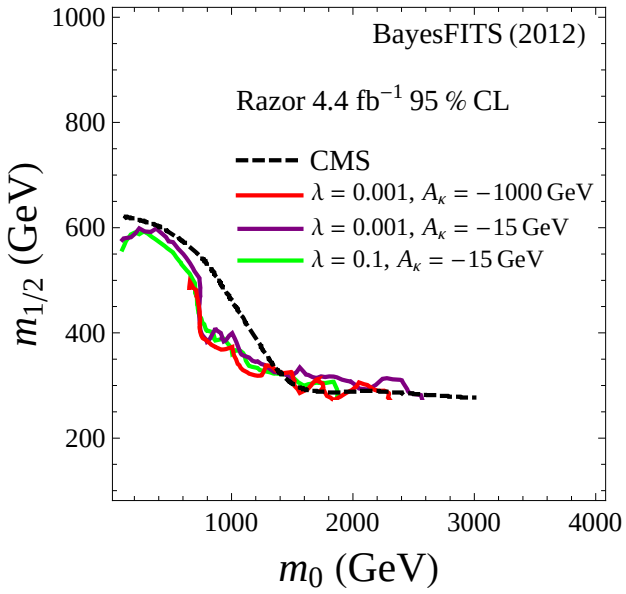

Figure 1: The 95% CL lower bounds from our approximate razor likelihood, for different values of λ and A_κ, compared with the experimental line (in dashed black).

by CMS is also shown as a dashed black line. The relevant CNMSSM parameters were fixed as: $\tan\beta = 5$, $A_0 = 0$, $A_\kappa = -15\,\text{GeV}$, $\lambda = 0.001$ and $\text{sgn}(\mu_{\text{eff}}) = +1$. The produced line is indicated in purple. One can see that the CMS limit is reproduced very well in the limits of $m_{1/2} \gg m_0$ and vice versa. A slight disrepancy in between those two extremes is basically irrelevant, as we shall see below. The dependence of the limit on λ and A_κ is negligible, since these parameters only affect the boundaries of the physically allowed region but do not cause a shift in the position of the contour. This is clear from Fig. 1, where we show a contour for $\lambda = 0.1$ (in green) and another for $A_\kappa = -1000\,\text{GeV}$ (in red), fixing the other parameters to the stated value in each case. The negligible dependence of the razor limit on A_0, $\tan\beta$ and $\text{sgn}(\mu_{\text{eff}})$ has already been verified in many analyses; see e.g., [56, 57, 29]. Our choice of these parameters thus only ensures maximum allowed physical region in the (m_0, $m_{1/2}$) space, since the physicality aspect is later taken into account during the scan when the unphysical points are discarded.

3.3 Likelihood for the Higgs bosons

The measured mass of the Higgs-like boson has important consequences for global properties of the CNMSSM.

The upper limit on the mass of h_1 is given by [58]

$$m_{h_1}^2 \leq M_Z^2 \cos^2 2\beta + \lambda^2 v^2 \sin^2 2\beta - \frac{\lambda^2}{\kappa^2} v^2 \left[\lambda - \sin 2\beta \left(\kappa - \frac{A_\lambda}{2s}\right)\right]^2 + \Delta m_h^2, \tag{6}$$

where Δm_h^2 denotes loop corrections, and $v = 174\,\text{GeV}$ is the tree-level Higgs doublet vev. The second, NMSSM-induced term on the right-hand side of Eq.(6) can enhance the h_1 mass by a few GeV beyond its MSSM value, if λ is large enough, $\lambda \gtrsim 0.5$, and $\tan\beta \lesssim 2$. For larger values of $\tan\beta$, the second term on the right-hand side becomes suppressed, and the third, negative term becomes significant. Then, the value of the Higgs boson mass can only be enhanced by the loop corrections. As we shall see, when other constraints are taken into account, especially the ones

coming from the LEP Higgs searches, b-physics, the muon anomalous magnetic moment, $(g-2)_\mu$, and DM relic density, the aforementioned conditions on λ and $\tan\beta$ become hard to satisfy and drastically restrict the parameter space of the model.

As noted in the Introduction, in the NMSSM either of the two lightest CP-even Higgses could serve the role of the SM-Higgs-like boson observed at the LHC. There are thus three interesting possibilities entailing such a discovery:[2]

Case 1: $m_{h_1} \simeq 125.8\,\text{GeV}$,
Case 2: $m_{h_2} \simeq 125.8\,\text{GeV}$,
Case 3: $m_{h_1} \simeq m_{h_2} \simeq 125.8\,\text{GeV}$.

3.3.1 Mass Likelihood

In this paper we analyze all the three cases mentioned above. We will henceforth refer to our selected 125.8 GeV signal Higgs for either of the first two cases generically as $h_{\rm sig}$. We impose a mass requirement on $h_{\rm sig}$ through a Gaussian likelihood which takes into account both the theoretical (τ) and experimental (σ) errors, following the procedure detailed in Ref. [29],

$$\mathcal{L}_{\text{Higgs mass}}(m_{h_{\rm sig}}) = \exp\left[-(125.8\,\text{GeV} - m_{h_{\rm sig}})^2/2(\tau^2+\sigma^2)\right]\,. \tag{7}$$

The theoretical error is due to residual differences between calculations using different approaches and schemes, and it is estimated in the literature to be of the order of $2-3\,\text{GeV}$ [59]. We assume $\tau = 3\,\text{GeV}$. We use the CMS determination of the Higgs mass rather than the one by ATLAS, since it has been most recently updated, and also for consistency with our previous work [29].

3.3.2 Cross section Likelihood

In order to be thoroughly consistent with the CMS measurement, we need to calculate for both Higgs bosons $h_{1,2}$ the reduced cross sections, defined in the literature as

$$R_{h_i}(X) = \frac{\sigma(pp\to h_i)}{\sigma(pp\to h_{\rm SM})} \times \frac{BR(h_i\to X)}{BR(h_{\rm SM}\to X)}\,, \tag{8}$$

for a given Higgs decay channel, X.

Equation (8) can be approximated by

$$R_{h_i}(X) = \sum_{Y\in\text{ prod}} R^Y_{h_i}(X)\mathcal{R}_{\rm SM}(Y)\,, \tag{9}$$

where the sum runs over the Higgs production channels Y ($Y = gg$ for gluon-fusion, VV for vector boson-fusion and Higgs-strahlung off a Z boson, $t\bar{t}$ and $b\bar{b}$ for associated Higgs production with top and bottom quarks, respectively), and the ratios $\mathcal{R}_{\rm SM}(Y) \equiv \sigma(pp\to Y\to h_{\rm SM})/\sigma(pp\to h_{\rm SM})$ are obtained from the public tables provided by the LHC Higgs Cross Section Working Group [60, 61] for $\sqrt{s} = 8\,\text{TeV}$.

The reduced cross sections $R^Y_{h_i}(X)$ for the individual production channels are provided by the mass spectrum generator, NMSSMTools, that we use for our analysis. Alternatively, they can be expressed in terms of the Higgs reduced couplings $C(X)$ (the ratio of the couplings of the Higgs boson with a given mass to a pair of X particles in the NMSSM, to the ones calculated in the

[2] We assume that the third CP-even Higgs is always heavier than the current experimental reach.

SM) and the decay branching ratios $\mathrm{BR}(h_i \to X)$, which are also provided by the mass spectrum generator,

$$\begin{aligned} R^Y_{h_i}(X) &\equiv \frac{\sigma(Y \to h_i)}{\sigma(Y \to h_{\rm SM})} \times \frac{\mathrm{BR}(h_i \to X)}{\mathrm{BR}(h_{\rm SM} \to X)} \\ &= C^2(Y) \times \frac{\Gamma(h_i \to X)/\Gamma_{\rm tot}}{\Gamma(h_{\rm SM} \to X)/\Gamma^{\rm SM}_{\rm tot}} \\ &= C^2(Y) C^2(X) \sum_{F \in \text{ SM decay}} \frac{\mathrm{BR}(h_i \to F)}{C^2(F)}\,, \end{aligned} \tag{10}$$

where the sum runs over the decay channels F open to the SM Higgs boson.

We require $R_{h_{\rm sig}}(\gamma\gamma)$ and $R_{h_{\rm sig}}(ZZ)$ to comply with the measured rates, $R_{\rm obs}(\gamma\gamma) = 1.6 \pm 0.4$ [1] and $R_{\rm obs}(ZZ) = 0.8^{+0.35}_{-0.28}$ [4], respectively.[3] For the $\gamma\gamma$ channel the 'signal' likelihood is taken to be a Gaussian around the measured central value,

$$\mathcal{L}_{\rm sig}(\gamma\gamma) = \exp\left[-\left(R_{\rm obs}(\gamma\gamma) - R_{h_{\rm sig}}(\gamma\gamma)\right)^2 / 2(\sigma^2_{\gamma\gamma} + \tau^2_{\gamma\gamma}) \right], \tag{11}$$

with $\sigma_{\gamma\gamma}$ being the experimental error. For the ZZ channel, since the experimental error is asymmetric, the signal likelihood is defined in terms of half-Gaussians for the positive error σ^+_{ZZ} and negative error σ^-_{ZZ} each, as done in the case of the $B_s \to \mu^+\mu^-$ likelihood above. $\tau_X \sim 15\% \times R_{h_{\rm sig}}(X)$, is a very conservative estimate of the theoretical error based on [62], used for every channel X.

In addition to constraining $h_{\rm sig}$, there is another crucial aspect of the Cases 1 and 2, which is that the second of the two lightest CP-even Higgs bosons must have escaped detection at the LHC, or be 'hidden'. In the following we refer to it as $h_{\rm hid}$. In other words, the production rate of $h_{\rm hid}$ should be less than what the experiments are currently sensitive to for all X. As a result, $R_{h_{\rm hid}}(X)$ should also be constrained by experimental data, so that all points where the rate of $h_{\rm hid}$ is large enough for it to have been observed, are rejected in our analysis. For this purpose, we construct an 'exclusion' likelihood. Following the procedure outlined in [48] for exclusion bounds we first define a step function,

$$\mathcal{L}^{\rm (step)}_{\rm excl}\left(m_{h_{\rm hid}}, R_{h_{\rm hid}}(X), \mu_{95}(X)\right) = \begin{cases} 1 & \text{for } R_{h_{\rm hid}}(X) \le \mu_{95}(X) \\ 0 & \text{for } R_{h_{\rm hid}}(X) > \mu_{95}(X), \end{cases} \tag{12}$$

where $\mu_{95}(X)$ is the value of the *signal strength modifier* $\mu(X) \equiv \sigma_{h_{\rm hid}}(X)/\sigma_{h_{\rm SM}}(X)$ that is excluded at 95% CL by the LHC searches for a Higgs with a given mass $m_H = m_{h_{\rm hid}}$, obtained from the latest exclusion plots published by the CMS collaboration [63].[4] Then, in order to take into account the theoretical error on the true values of the reduced cross section and the Higgs mass, $\mathcal{L}^{\rm (step)}_{\rm excl}$ is smeared out further by convolving it with Gaussian functions centered around their true theoretical values $\hat{R}_{h_{\rm hid}}(X)$ and $\hat{m}_{h_{\rm hid}}$, respectively, so that the exclusion likelihood now becomes

$$\begin{aligned} \mathcal{L}^{\rm (smear)}_{\rm excl}\left(m_{h_{\rm hid}}, R_{h_{\rm hid}}, \mu\right) = \int d\hat{m}_{h_{\rm hid}} \int d\hat{R}_{h_{\rm hid}}\, \mathcal{L}^{\rm (step)}_{\rm excl}\big(\hat{m}_{h_{\rm hid}}, \hat{R}_{h_{\rm hid}}, \mu\big) \\ \times \exp\left[-\frac{(\hat{m}_{h_{\rm hid}} - m_{h_{\rm hid}})^2}{2\tau^2} \right] \exp\left[-\frac{(\hat{R}_{h_{\rm hid}} - R_{h_{\rm hid}})^2}{2\tilde{\tau}^2} \right], \end{aligned} \tag{13}$$

[3] We only use the dominant decay channels where a $\sim 5\sigma$ excess has been observed.

[4] We used the latest exclusion limits provided based on 5.1/fb of data at $\sqrt{s} = 7\,\mathrm{TeV}$ and 12.2/fb of data at $\sqrt{s} = 8\,\mathrm{TeV}$ for the ZZ channel, on 4.9/fb at $\sqrt{s} = 7\,\mathrm{TeV}$ and 12.1/fb at $\sqrt{s} = 8\,\mathrm{TeV}$ for the $WW \to ll\nu\nu$ channel and on 17/fb at $\sqrt{s} = 7 - 8\,\mathrm{TeV}$ for the $\tau\tau$ channel. Limits for the $\gamma\gamma$ channel have not been updated by CMS and are, therefore, still based on a combination of 5.1/fb at $\sqrt{s} = 7\,\mathrm{TeV}$ and 5.3/fb at $\sqrt{s} = 8\,\mathrm{TeV}$ of data.

CNMSSM parameter	Description	Prior Range	Prior Distribution
m_0	Universal scalar mass	100, 4000	Log
$m_{1/2}$	Universal gaugino mass	100, 2000	Log
A_0	Universal trilinear coupling	-7000, 7000	Linear
$\tan\beta$	Ratio of Higgs vevs	1, 62	Linear
λ	Higgs trilinear coupling	0.001, 0.7	Linear
Nuisance	Description	Central value $\pm$ std. dev.	Prior Distribution
M_t	Top quark pole mass	173.5 ± 1.0	Gaussian
$m_b(m_b)^{\overline{MS}}$	Bottom quark mass	4.18 ± 0.03	Gaussian
$\alpha_s(M_Z)^{\overline{MS}}$	Strong coupling	0.1184 ± 0.0007	Gaussian

Table 2: Priors for the parameters of the model and for the SM nuisance parameters used in our scans. Masses and A_0 are in GeV.

where the theoretical errors are taken to be $\tau = 3\,\text{GeV}$ and $\tilde{\tau} = 15\% \cdot R_{h_{\text{hid}}}$ [62], respectively. The exclusion likelihood is calculated for $X = \gamma\gamma$, ZZ, WW and $\tau\tau$. Finally, in order for our exclusion criterion to be consistent with our criterion for signal observation at $125.8 \pm 3.1\,\text{GeV}$ (with theory and experimental errors added in quadrature), we further impose the condition

$$\mathcal{L}_{\text{excl}}(X) = \begin{cases} 0 & \text{for } 122.7\,\text{GeV} \leq m_{h_{\text{hid}}} \leq 128.9\,\text{GeV} \\ \mathcal{L}_{\text{excl}}^{(\text{smear})}(X) & \text{elsewhere.} \end{cases} \tag{14}$$

For Case 3, the likelihood in Eq. (7) is separately computed for both h_1 and h_2. In this scenario, only the combined production rate for h_1 and h_2 needs to be equal to $R_{\text{obs}}(X)$. Hence the observation likelihood is now defined as

$$\mathcal{L}_{\text{obs}}(X) = \exp\left\{ -\left[R_{\text{obs}}(X) - (R_{h_1}(X) + R_{h_2}(X))\right]^2 / 2(\sigma_X^2 + \tau_X^2) \right\}. \tag{15}$$

The values and uncertainties of our Higgs constraints are given in Table 1.

4 Methodology and Results

The scanned ranges of the CNMSSM parameters along with the type of distribution of their prior are listed in Table 2. Also listed there are the input ranges of the nuisance parameters included in the scans. The sign of μ_{eff} is fixed for a given scan and equal to $+1$ or -1.

The analysis was performed using the package BayesFITS which engages several external, publicly available tools: for sampling it uses MultiNest [64] with 4000 living points, evidence tolerance factor set to 0.5, and sampling efficiency equal to 0.8. Mass spectrum, along with ΔM_{B_s}, is computed with NMSSMTools v3.2.1 and passed via SUSY Les Houches Accord format to SuperIso v3.3 [65] to calculate $\text{BR}\left(\overline{\text{B}} \to \text{X}_\text{s}\gamma\right)$, $\text{BR}\left(\text{B}_\text{s} \to \mu^+\mu^-\right)$, $\text{BR}\left(\text{B}_\text{u} \to \tau\nu\right)$, and $\delta\left(g-2\right)_\mu^{\text{SUSY}}$. DM observables, such as the relic density and direct detection cross sections, are calculated with MicrOMEGAs 2.4.5 [66].

Below we will present the results of our scans as one-dimensional (1D) or two-dimensional (2D) marginalized posterior pdf maps of parameters and observables. For example, in evaluating a posterior pdf for a given parameter, we marginalize over the model's all other parameters and the SM nuisance parameters, as described in detail in Refs. [29, 41].

Notice that when discussing the results of the global scan for Case 1 it will become apparent that this case presents a remarkable CMSSM-like behavior. It would therefore be natural to try to

compare those results with our recent CMSSM analysis [29]. In doing so, one needs to take into account the differences between the numerical codes and constraints adopted in both studies. We summarize them here.

1. In the present study we use NMSSMTools for calculating the supersymmetric spectrum, while in [29] we used SoftSUSY. We have repeatedly cross-checked the spectra obtained in the MSSM limit of the NMSSM with the ones generated by SoftSUSY, finding some differences, especially with respect to loop corrections giving the largest values of the lightest Higgs mass. In some regions of the parameter space the difference between the two generators can amount to a maximum of ~ 0.5–$1\,\text{GeV}$.[5] Given the experimental and theoretical uncertainties in the Higgs mass, such difference translates into ~ 0.25 units of χ^2, which is not significant for the purpose of the global scan.

2. In this paper we use the value of $\text{BR}\,(\text{B}_\text{s} \to \mu^+\mu^-)$ measured at LHCb [35], which has been incorporated in the likelihood as described is Sec. 3.1. The SM rate rescaled by the time dependent asymmetries is now $\text{BR}\,(\text{B}_\text{s} \to \mu^+\mu^-)_\text{SM} = (3.53 \pm 0.38) \times 10^{-9}$ [50], which is a value more appropriate for comparison with the experimental rate than the unscaled, $\sim 3.2 \times 10^{-9}$, one.

3. We have updated the nuisance parameters M_t and $m_b(m_b)^{\overline{MS}}$ following [38]; see Table 2. The upgrade in M_t has significant implications for m_{h_1}. The leading one-loop corrections to the Higgs mass squared are given by

$$\Delta m_h^2 = \frac{3m_t^4}{4\pi^2 v^2}\left[\ln\left(\frac{M_\text{SUSY}^2}{m_t^2}\right) + \frac{X_t^2}{M_\text{SUSY}^2}\left(1 - \frac{X_t^2}{12M_\text{SUSY}^2}\right)\right], \tag{16}$$

where m_t is the running top quark mass,[6] M_SUSY is the geometrical average of the physical stop masses, $M_\text{SUSY} \equiv \sqrt{m_{\tilde{t}_1} m_{\tilde{t}_2}}$, and $X_t = A_t - \mu_\text{eff} \cot\beta$. Since $\Delta m_h^2 \propto m_t^4$ it is now easier to generate Higgs masses in agreement with the experimental values. In particular, as we highlighted in [29], a Higgs mass compatible with the observed excess at $126\,\text{GeV}$ was rather difficult to achieve over the CMSSM parameter space. That tension has now become somewhat reduced, and we will show below that the correct Higgs mass can be obtained in the CMSSM limit of the CNMSSM.

4.1 Impact of the relic density

To set the ground for the presentation of our numerical results, we first comment on the role of the relic density of DM in selecting favored regions. The relic density is a strong constraint, since it is a positive measurement (in contrast to a limit) with a rather small experimental uncertainty (Table 1). On top of it, it is well known that in unified SUSY models with neutralino LSP the corresponding abundance $\Omega_\chi h^2$ is typically too large, or in other words, its annihilation in the early Universe is 'generically' too inefficient. Specific mechanisms for enhancing it are therefore needed which, however, are only applicable in specific SUSY configurations. As a result, in most cases the regions of high probability in the global posterior will reflect one or more of the regions of parameter space where $\Omega_\chi h^2$ is close to the measured relic density of DM. The regions that are still allowed by direct SUSY searches are:

1. The stau-coannihilation (SC) region [68]. As is known, in constrained SUSY models, like the C(N)MSSM, this is a narrow strip at a sharp angle to the $m_{1/2}$ axis. The values of A_0 and $\tan\beta$ are also constrained, as only for $|A_0|$ not exceeding $\sim$2–3 TeVand $\tan\beta$ not too large does the mass of the stau become light enough to be comparable with the neutralino mass, but not too light so to make it the LSP. Values of $m_{1/2}$ that are excessively large, on the other hand,

[5] The best agreement between SoftSUSY and NMSSMTools is obtained by setting the flag `precision for the Higgs masses` to zero which, therefore, was chosen as default setting for our calculations.

[6] Note that running top quark mass is related to the pole mass through the formula given in Eq. (10) of Ref. [67].

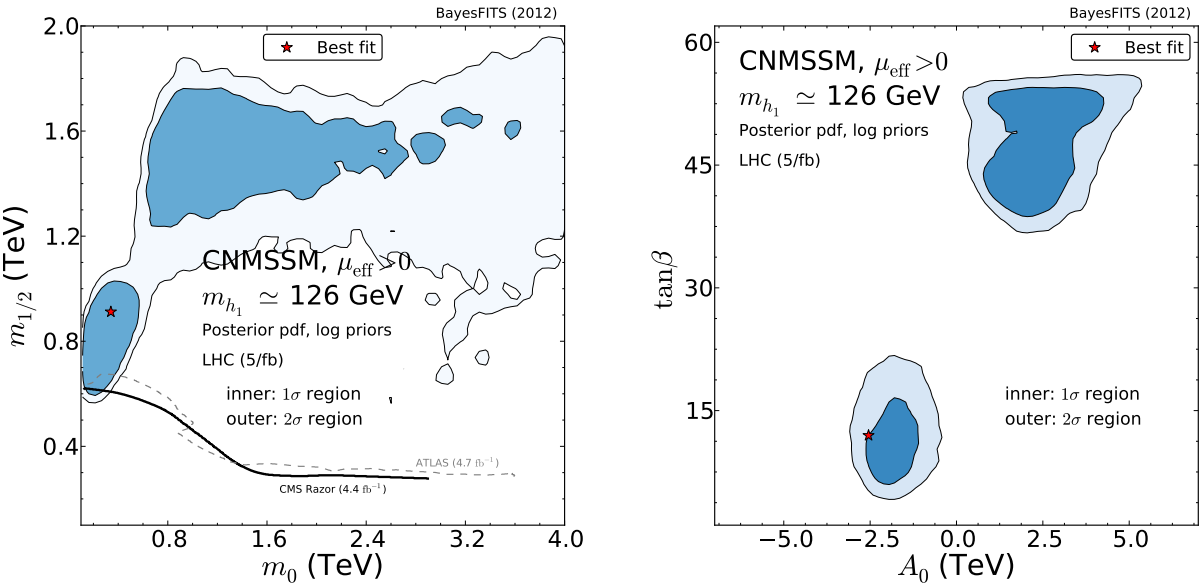

(a) (b)

Figure 2: Marginalized 2D posterior pdf in (a) the (m_0, $m_{1/2}$) plane and (b) the (A_0, $\tan\beta$) plane of the CNMSSM for Case 1, constrained by the experiments listed in Table 1. The 68% credible regions are shown in dark blue, and the 95% credible regions in light blue. The solid black (dashed gray) line shows the CMS razor (ATLAS hadronic) 95% CL exclusion bound.

can suppress the annihilation cross section [69]. After other relevant constraints are included, the parameters of interest are, therefore, $m_0 \lesssim 600\,\text{GeV}$, $m_{1/2} \lesssim 1000\,\text{GeV}$, $|A_0| \lesssim 3000\,\text{GeV}$ and, when the neutralino is close to 100% bino, $\tan\beta < 30$. A similar effect can also be obtained for large A_0 with the stop $\tilde{t}_1$ replacing $\tilde{\tau}_1$ [70].

2. The A-funnel (AF) region, where neutralinos annihilate through the resonance with the lightest pseudoscalar [71]. This mechanism can occur over broad ranges of the (m_0, $m_{1/2}$) plane where the pseudoscalar mass is close to twice the neutralino LSP mass, and is enhanced by large $\tan\beta$ ($\tan\beta \gtrsim 35$) and positive A_0.

3. The focus point/hyperbolic branch (FP/HB) region [72, 73], where the annihilation cross section can be enhanced by an increased higgsino component of the neutralino. For this to occur, μ (or $\mu_{\rm eff}$ in the NMSSM) must be of the order of a few hundred GeV, and $\tan\beta$ cannot be too large, $\tan\beta \lesssim 45$. In the (m_0, $m_{1/2}$) plane the condition corresponds to the region where $m_0 \gg m_{1/2}$.

4.2 Impact of the Higgs mass

The measurement of the Higgs mass has added an important additional constraint on unified SUSY models. Below we will be discuss in turn the three cases listed earlier in Sec. 3.3.

Case 1. In Fig. 2(a) we show the marginalized posterior pdf in the (m_0, $m_{1/2}$) plane of the CNMSSM for Case 1, obtained by imposing simultaneously all the constraints shown in Table 1. In these and the following plots the Bayesian 68% (1σ) credible regions are indicated in dark blue and the 95% (2σ) credible regions in light blue. Notice that the regions of high probability are located above the CMS razor limit, which we implemented in the likelihoood as described in Sec. 3.2, and

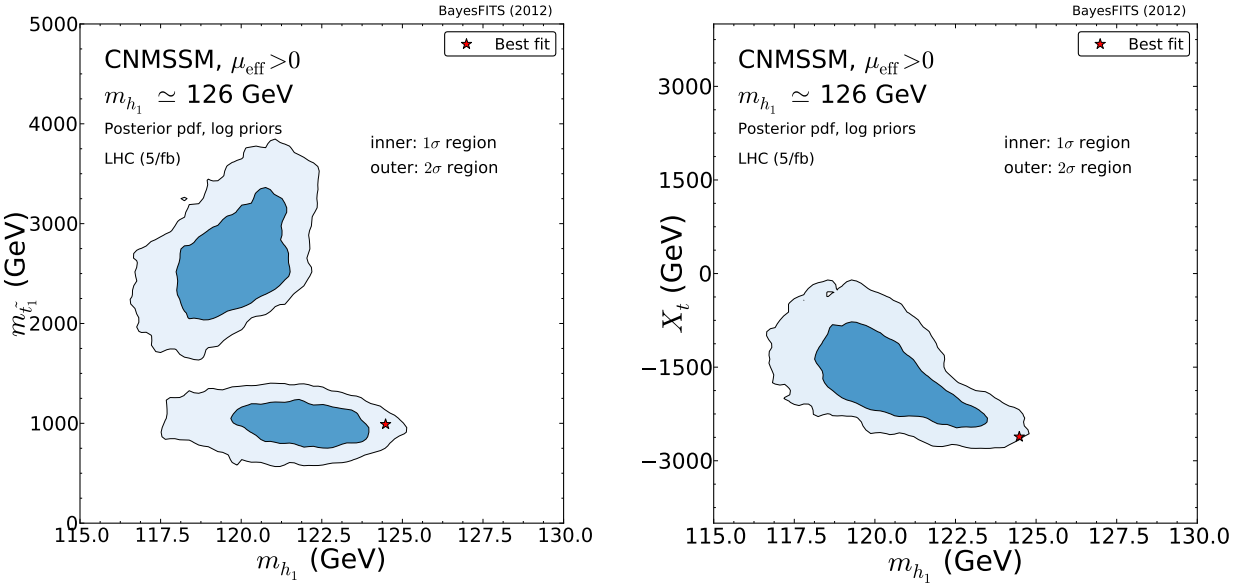

(a) (b)

Figure 3: Marginalized 2D posterior pdf in (a) the (m_{h_1}, $m_{\tilde{t}_1}$) plane and (b) the (m_{h_1}, X_t) plane, for the CNMSSM constrained by the experiments listed in Table 1 for Case 1. The color code is the same as in Fig. 2.

which is shown in the plots as a solid black line. In Case 1 the role of the SM-like Higgs is played by the lightest CP-even scalar (almost purely H_u^0-like), while h_2 (almost purely H_d^0-like) and h_3 (almost purely singlet-like) are usually much heavier and decoupled. This case is thus expected to present features very similar to the CMSSM.

In Fig. 2(a) one can see two main 68% credibility regions: the SC region on the lower left side, and the AF region on the top part of the plot. As is also the case in the CMSSM, besides giving the correct relic abundance, the SC region shows also the better fit to the Higgs mass, $m_{h_1} = 124.5\,\text{GeV}$. This is because, as we explained in Ref. [29], in the SC region A_0 can easily be negative without spoiling the relic abundance constraint. Large negative values of A_0 are necessary to drive the parameter A_t to even larger negative values at the EW scale, thus making the stop mixing contribution to the loop corrections of the Higgs mass maximal. Note as well that the best-fit point is also located in the SC region.[7] In Fig. 2(b) we show the marginalized posterior in the (A_0, $\tan\beta$) plane. The high probability 'island' at negative A_0 and $\tan\beta \lesssim 25$ corresponds to the SC region.

In the CNMSSM the SC region appears to be more extended relative to the CMSSM [29], and somewhat larger Higgs masses also seem allowed, as we will show below. The increased relevance of the SC region is due to the fact that it is now much easier to obtain values of the Higgs mass closer to the correct one. This could be mistakenly thought to be a specific feature of the CNMSSM extended Higgs sector. We have checked that this is not the case: the Higgs mass is simply quite sensitive to the increased central value of the top mass, as we explained at the beginning of this section.

In Figs. 3(a) and 3(b), we show how the constraints affect the main observables responsible for

[7] We postpone further discussion of the best-fit points until Sec. 4.7.

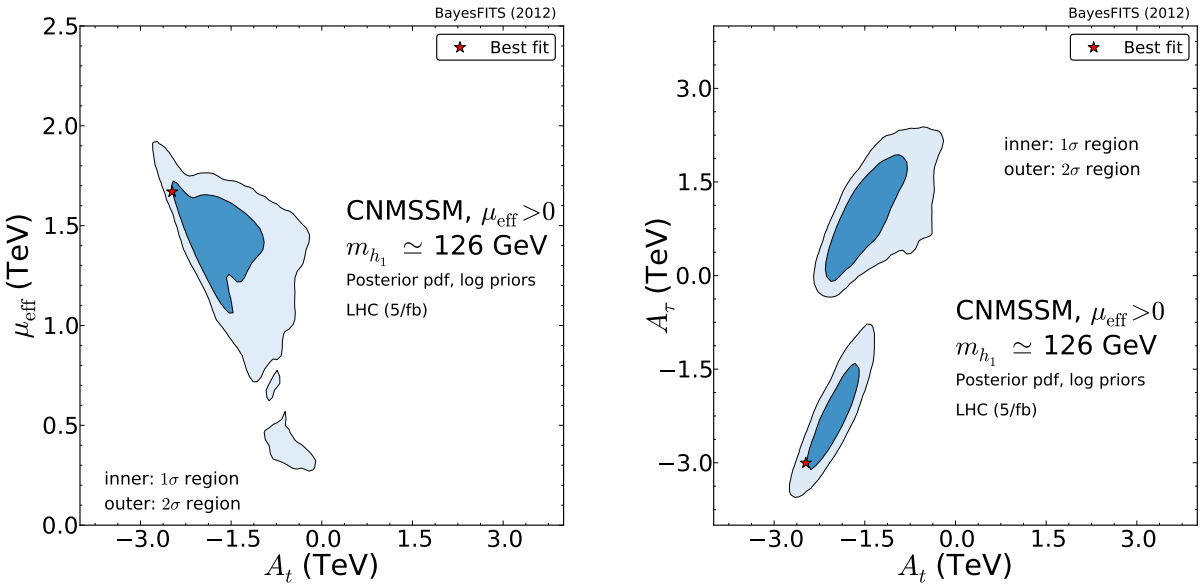

(a) (b)

Figure 4: Marginalized 2D posterior pdf in (a) the (A_t, $\mu_{\rm eff}$) plane and (b) the (A_t, A_τ) plane, for the CNMSSM constrained by the experiments listed in Table 1 for Case 1. The color code is the same as in Fig. 2.

the loop corrections to the Higgs boson mass. In Fig. 3(a), we show the posterior in the (m_{h_1}, $m_{\tilde{t}_1}$) plane. Notice that the lightest stop *does not need to be excessively heavy* in the SC region, $m_{\tilde{t}_1} \sim 1\,\text{TeV}$, since large stop mixing compensates for smaller $M_{\rm SUSY}$. The correct Higgs mass is obtained since $|X_t| \sim 2.5\,\text{TeV}$, as can be seen in Fig. 3(b) where we plot the posterior in the (m_{h_1}, X_t) plane. On the other hand, one can see that in both figures the best-fit point lies outside of the 68% credibility regions of the marginalized 2D pdf, when the latter is projected to the plane of these observables. This is a feature not uncommon in Bayesian analyses where the credibility regions map the 'volume' of scan points satisfying well enough a certain set of constraints, rather than representing iso-contours of the likelihood function, as is the case in frequentist analyses. The fact that the best-fit point is situated outside of the region of highest posterior probability for the considered observables simply tells us that, while for this point all the constraints are very well satisfied, it is also not very likely to obtain a similarly good value of the observable for similar choices of the input parameters. Particularly, in the case of Figs. 3(a) and 3(b), the majority of the points that satisfy all the constraints in the SC region present a Higgs mass in the range 120–123 GeV, while for the other regions it is even less.

Figure 2(a) also shows that the Higgs mass constraint favors the part of the AF region situated at $m_{1/2} \gtrsim 1500\,\text{GeV}$ for a broad range of m_0 values. Besides, in Fig. 2(b) one can see that in the (A_0, $\tan\beta$) plane the AF region spans a large range of positive A_0 values and $\tan\beta$ is constrained to $\tan\beta \gtrsim 40$. In this region one loop corrections to the Higgs mass are driven up by a large stop mass ($m_{\tilde{t}_1} \sim 2-4\,\text{TeV}$, as shown in Fig. 3(a)) rather than large stop mixing which, given the allowed values of A_0, is minimal (see Fig. 3(b)). Large values of $M_{\rm SUSY}$ push the Higgs mass close to the experimentally observed value, but not enough to reach it (for even larger $M_{\rm SUSY}$, m_{a_1} becomes too heavy and resonant annihilation of neutralinos is not efficient). This can be interpreted as a sign

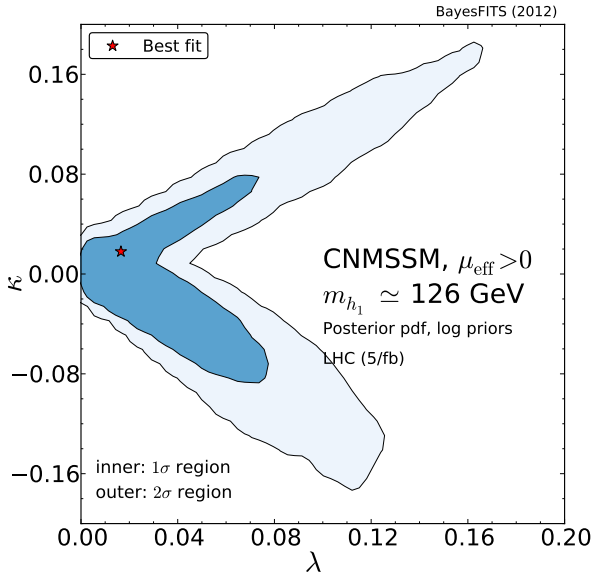

Figure 5: Marginalized 2D posterior pdf in the (λ, κ) plane, for the CNMSSM constrained by the experiments listed in Table 1 for Case 1. The color code is the same as in Fig. 2.

of some tension between the relic abundance and Higgs mass constraints in the AF region, which was investigated for the CMSSM in our previous paper [29]. The tension persists in the CNMSSM.

Only a limited fraction of the FP/HB region (which appears as a narrow 95%-credibility 'tail' at $m_0 \gg m_{1/2}$) survives, as was the case for the CMSSM, despite the fact that the relic density is well satisfied over there. As we pointed out in [29], some tension with the 126-GeV Higgs boson mass arises not only in the AF but also in the FP/HB region where $\mu_{\rm eff}$ is smaller than anywhere else. In fact, small values of $\mu_{\rm eff}$ do not allow to obtain large negative A_t through running, as can be seen in Fig. 4(a), where we show the posterior in the weak scale parameters A_t and $\mu_{\rm eff}$ (notice that $A_t \simeq X_t$ over all parameter space). For the chosen range of m_0, in the FP/HB region $M_{\rm SUSY}$ cannot be very large either, so that the correct Higgs mass cannot be reached. The region of high posterior thus moves up towards larger $m_{1/2}$, where the neutralino has still a non-negligible higgsino component, but $M_{\rm SUSY}$ is large enough to give the correct Higgs mass.

It is worth pointing out that $A_0 \sim 0$ is not realized in the CNMSSM. This is because the lightest pseudoscalar a_1 becomes non-physical for such values. The mass of a_1 is, for moderate and large values of $\tan\beta$, well approximated by $m^2_{a_1} \approx -3\kappa s A_\kappa$ [74]. A_λ and A_κ are unified to A_0 at the GUT scale, and A_κ barely runs, since the one-loop contribution to its β-function is negligible. As a consequence, in the CNMSSM κ and A_κ have always opposite signs and there are no points in the scan with $A_0 = 0$ or $\kappa = 0$.

We present in Fig. 4(b) the marginalized posterior pdf in the (A_t, A_τ) plane. The parameters show a clear linear correlation, which in the SC region (bottom left corner) results in large negative values for both observables, due to the fact that the correct Higgs boson mass requires large stop mixing, as discussed above.

Figure 5 shows the 2D-posterior in the (λ, κ) plane. One can notice the known correlation between κ and λ [31], as $|\kappa|$ cannot exceed a given value of λ by too much without causing a Landau pole in RGE running and, on the other hand, λ cannot exceed a given value of $|\kappa|$ by too much without lowering m_{h_1} much below the observed value, where the likelihood becomes

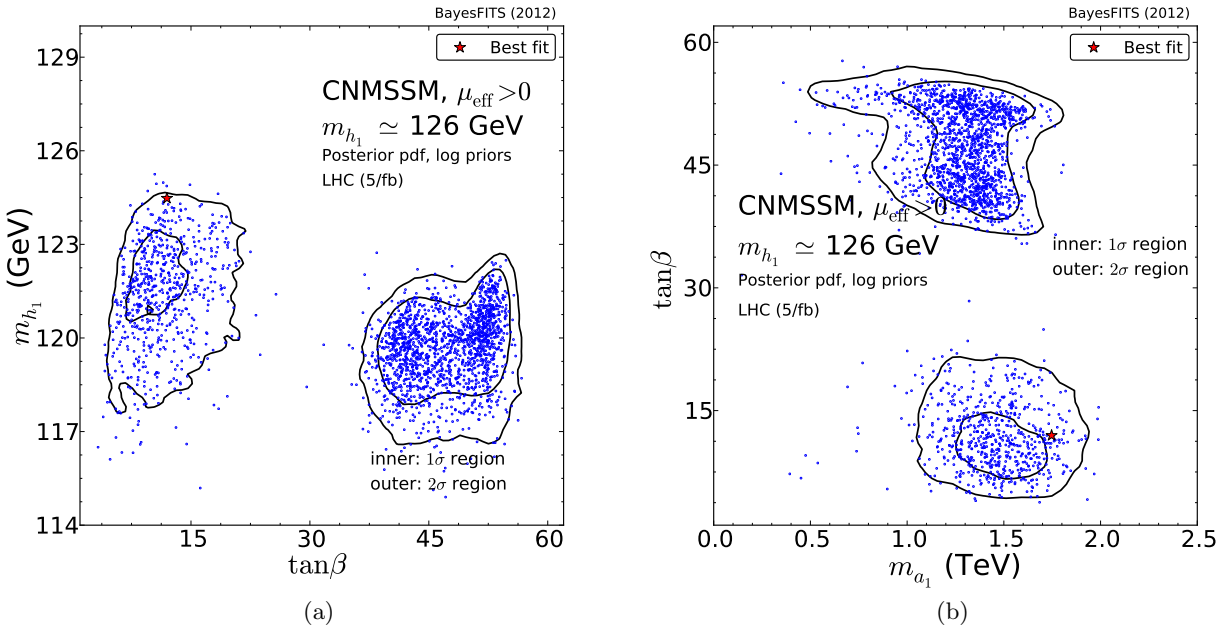

Figure 6: Marginalized 2D posterior pdf in (a) the ($\tan\beta$, m_{h_1}) plane and (b) the (m_{a_1}, $\tan\beta$) plane of the CNMSSM constrained by the experiments listed in Table 1 for Case 1. The outer contours enclose the 95% credibility regions and the inner contours the 68% credibility regions. A distribution of samples uniformly selected from our nested sampling chain is superimposed.

negligible. In the SC region κ is positive since A_κ is negative, while in the AF and FP/HB regions these parameters switch signs. Hence, the upper branch shown in Fig. 5 corresponds to the SC region, and the lower one to both the AF and the FP/HB regions.

At 95% credibility, λ and κ show an upper bound, which changes over parameter space depending on the value of $\mu_{\rm eff}$ and loop corrections to m_{h_1}, and again is due to the requirement of $m_{h_1} \sim 126\,\text{GeV}$. When all the constraints are taken into account, the posterior shows that $\lambda \lesssim 0.16$ for the upper branch, corresponding to the SC region, and $\lambda \lesssim 0.12$ for the lower branch corresponding to the AF and the FP/HB regions.

We want to re-emphasize that, when the global constraints are considered, Case 1 presents a very CMSSM-like character. The parameter λ is small, and its effect on m_{h_1} is insignificant, given that $\tan\beta \gtrsim 4$ over all of the regions of high posterior probability, as shown in Fig. 2(b). In the SC region the lightest Higgs mass can assume values close to 126 GeV more easily than what was observed in our work on the CMSSM, but the reason lies in the updated value of the top mass used for the present analysis.

In Fig. 6(a) we show the marginalized posterior in the ($\tan\beta$, m_{h_1}) plane and in Fig. 6(b) the posterior in the (m_{a_1}, $\tan\beta$) plane. We also overlap a distribution of samples uniformly selected from our nested sampling chain. Notice that the density of samples reflects their relative posterior probability. One can see in Fig. 6(a) that, in the SC region (left island) the tension between the correct Higgs mass and the other constraints is much ameliorated. Figure 6(b) shows confirmation of the CMSSM-like nature of this case, as the pattern of high posterior mirrors the one found in Ref. [29].

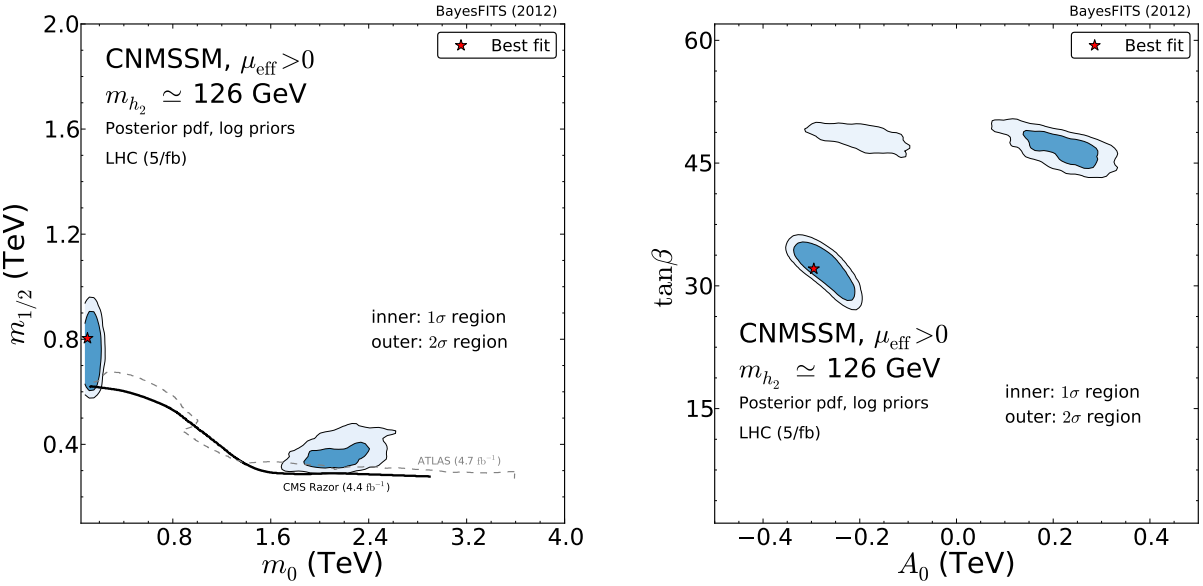

(a) (b)

Figure 7: Marginalized 2D posterior pdf in (a) the (m_0, $m_{1/2}$) plane and (b) the (A_0, $\tan\beta$) plane of the CNMSSM constrained by the experiments listed in Table 1 for Case 2. The color code is the same as in Fig. 2.

Case 2. The NMSSM allows more freedom in the Higgs sector than the MSSM, due to the extended number of parameters. Even in its partially constrained version, there is a possibility of obtaining a light h_2, which we found to be a mixture of H_u and S fields. A non-negligible singlet component creates the difference in the Higgs sector between this scenario and Case 1. In the rest of this section we analyze the consistency of an h_2 signal with the observed excess at the LHC.

In Fig. 7(a) we show the posterior pdf in the (m_0, $m_{1/2}$) plane for Case 2. The favored parameter space is now drastically reduced with respect to Case 1. Only the SC region, where the best-fit point is located, and the FP/HB region survive the requirement of having $m_{h_2} \sim 126\,\text{GeV}$.

In Fig. 7(b) we show the posterior pdf in the (A_0, $\tan\beta$) plane. In both regions the range allowed for A_0 does not extend much from zero, $-400\,\text{GeV} < A_0 < 400\,\text{GeV}$.[8] The reason is that $|A_\kappa|$ is now limited to values less than 400 GeV by our requirement on the mass of h_2. Specifically, the masses of the two lightest CP-even Higgs bosons at the tree level are approximately given by [74]

$$m^2_{h_{1,2}} \approx \frac{1}{2}\left\{ M_Z^2 + 4(\kappa s)^2 + \kappa s A_\kappa \mp \sqrt{\left[M_Z^2 - 4(\kappa s)^2 - \kappa s A_\kappa\right]^2 + \lambda\text{-term}} \right\}, \tag{17}$$

where the λ-term under square root includes the usual correction to the tree level masses and depends on the other parameters of the Higgs sector. It is clear from Eq. (17), that in the regime where $|\kappa| s < M_Z$, the mass of h_2 is of order M_Z, while m_{h_1} scales as $|\kappa| s$. When m_{h_1} approaches zero, the λ-term is $\mathcal{O}(\lesssim 10^6\,\text{GeV})$, while the first term under square root is roughly of the order of $M_Z^4 \sim 10^8\,\text{GeV}$ or larger. The λ-term can therefore be neglected, and the requirement of having $m^2_{h_1} \geq 0$ translates into the approximate relation $|A_\kappa| \lesssim 4|\kappa| s$. On the other hand, in the regions where $|\kappa| s > M_Z$, $m_{h_2} \sim \kappa s$ and $m_{h_1} \sim M_Z$. Values of m_{h_2} much greater than 126 GeV are

[8] Note that a gap around $A_0 \sim 0$ in Fig. 7(b) comes from the physicality condition for a_1, as discussed above.

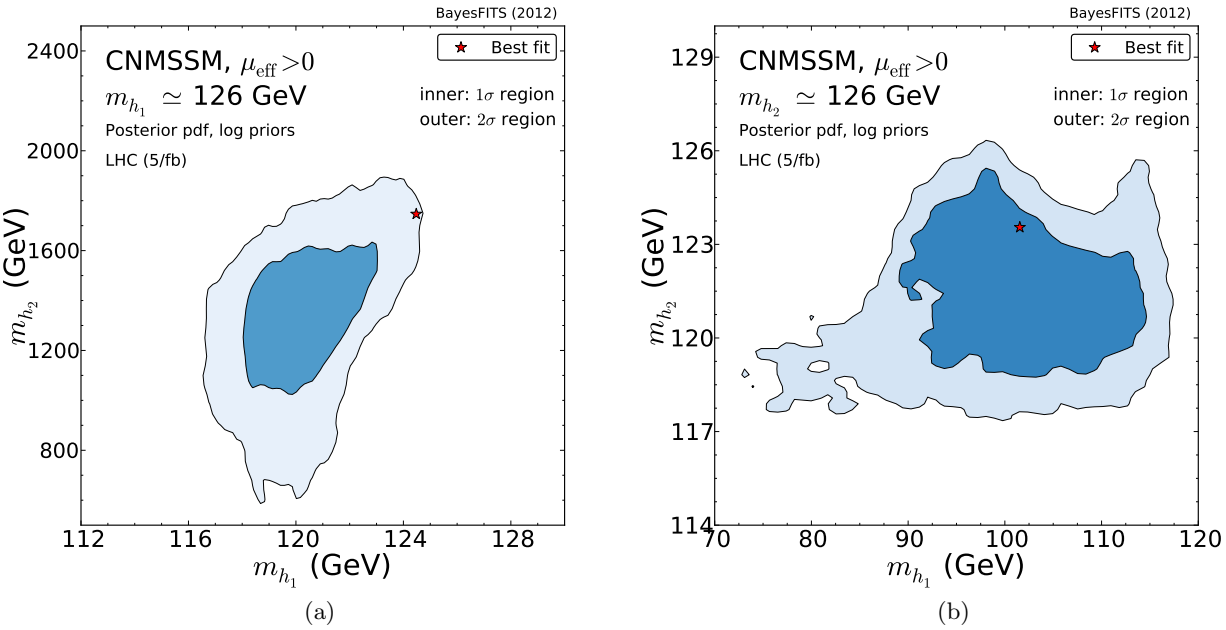

(a) (b)

Figure 8: (a) Marginalized 2D posterior pdf in the (m_{h_1}, m_{h_2}) plane of the CNMSSM constrained by the experiments listed in Table 1 for Case 1. (b) Marginalized posterior pdf in the (m_{h_1}, m_{h_2}) plane of the CNMSSM for Case 2. The color code is the same as in Fig. 2.

forbidden by the likelihood function, so that $|\kappa|s$ presents an upper bound, which translates into an upper bound on $|A_\kappa|$.

Since in most of the parameter space s is very large, and λ and κ are correlated, the scan also shows upper bounds for λ and κ. In the SC region λ is very small, $\lambda \lesssim 0.01$, while in the FP/HB region it can assume slightly larger values, $\lambda \lesssim 0.04$. Notice that the upper bound on $|\kappa|s$ does not depend on the other input parameters, but the bound on κ (or λ) does, particularly on the value of $\mu_{\rm eff}$. In the SC region $\mu_{\rm eff} > 600\,{\rm GeV}$ while in the FP/HB region $\mu_{\rm eff} \simeq 200\,{\rm GeV}$.

Since in the SC region λ and κ are bounded to be much smaller than in Case 1, the lightest neutralino there is *a nearly pure singlino* and very light (the neutralino mass matrix with the convention used in this paper can be found, e.g., in [31]). The corresponding $\tan\beta$ assumes larger values ($\tan\beta \sim 30-35$, favored also by other constraints, e.g. $\delta\,(g-2)_\mu$) than in the same region of Case 1, or of the CMSSM. For smaller values of $\tan\beta$, on the other hand, the lighter stau becomes the LSP.

In Figs. 8(a) and 8(b) we show the 2D posterior in the (m_{h_1}, m_{h_2}) plane for Case 1 and Case 2, respectively. One can see that in Case 1 $m_{h_2} \gg m_{h_1}$, while in Case 2 the 68% credibility region shows a preference for $90\,{\rm GeV} \lesssim m_{h_1} \lesssim 115\,{\rm GeV}$.

Since in Case 2 $m_{h_2} \sim 126\,{\rm GeV}$, m_{a_1} assumes values quite small in the favored regions, $m_{a_1} < 500\,{\rm GeV}$. While it might appear that such a case is excluded by the recent $H \to \tau\tau$ searches at the LHC [75], we point out that the limit does not apply to this case, as the relevant couplings for $a_1 \to \tau\tau$ and $a_1 \to bb$ are suppressed by the pseudoscalar mixing angle θ_P, i.e., when $|\cos\theta_P| < 1$ [76]. We have checked that $|\cos\theta_P|$ is very close to zero over the regions of interest.

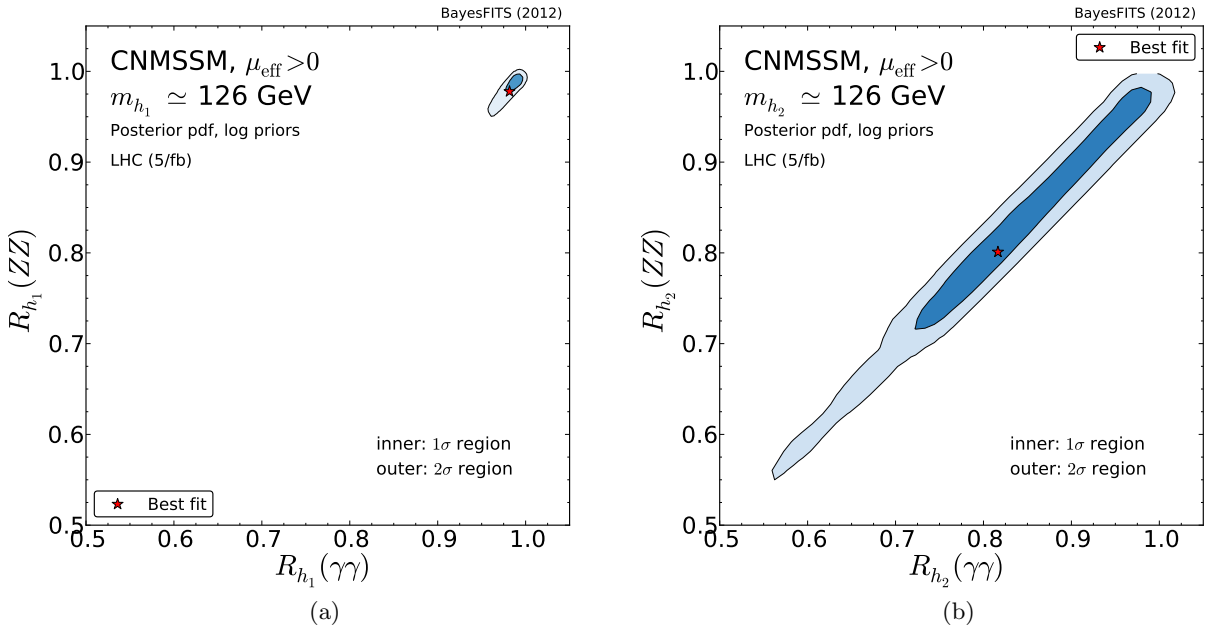

(a) (b)

Figure 9: (a) Marginalized 2D posterior pdf in the ($R_{h_1}(\gamma\gamma)$, $R_{h_1}(ZZ)$) plane of the CNMSSM constrained by the experiments listed in Table 1 for Case 1. (b) Marginalized posterior pdf in the ($R_{h_2}(\gamma\gamma)$, $R_{h_2}(ZZ)$) plane of the CNMSSM for Case 2. The color code is the same as in Fig. 2.

Case 3 (two degenerate light Higgs bosons) is in fact a subset of Case 2 when it comes to the allowed parameter space, which is uniquely determined by the requirement of $m_{h_2} \sim 126\,\text{GeV}$ as was explained above. The posterior pdf in this case is very similar to the one showed in Figs. 7(a) and 7(b), and the best-fit point is again situated in the SC region. However, this case presents also some characteristic features:

• h_1 is a mixture of H_d and H_u, with a predominance of the latter, while h_2 is mainly singlet-like, with a small fraction of H_d.

• Both λ and κ are now much more limited and very close to zero. The reason for this is simple: in order to have the two lightest CP-even Higgs bosons almost degenerated in mass, one needs to minimize the difference $m^2_{h_2} - m^2_{h_1}$ from Eq. (17). This yields negligible values for the parameter κ and, consequently, also for λ.

4.3 Impact of the cross section rates

In Fig. 9(a) we show the 2D posterior pdf in the ($R_{h_1}(ZZ)$, $R_{h_1}(\gamma\gamma)$) plane for Case 1. As one can see, the Higgs boson in this case is SM-like. Actually, it is known [30] that the enhancement of the signal strength in the $\gamma\gamma$ decay channel observed by both CMS and ATLAS cannot be obtained for the values of λ that are favored by the global scan. As a consequence, $R_{h_1}(\gamma\gamma)$ cannot be fitted perfectly in the CNMSSM. This discrepancy effectively adds two units of χ^2 homogeneously over the allowed parameter space, but it does not alter the posterior distribution. For the same reason $R_{h_1}(ZZ)$ cannot be perfectly fitted either, though its contribution to the total χ^2 is smaller than 0.5 units of χ^2, making this observable equally ineffective to constraining the posterior.

In Fig. 9(b) we present the posterior distribution for Case 2. Once again, $R_{h_2}(\gamma\gamma)$ can hardly become larger than one over the allowed parameter space. The 95% credible region lies far from

the central value of the observed enhancement and, in fact, even covers values lower than in Case 1. $R_{h_2}(ZZ)$ presents similar behaviour, although the suppression of the reduced cross section is highly welcome for this observable, as it places the calculated value closer to the rate observed at CMS. Smaller than one signal rates indicate less of a SM-like character for h_2, which is caused by the the suppression of the SM-couplings induced by its increased singlet component.

The posterior distributions presented in Figs. 9(a) and 9(b) indicate that, in both Case 1 and Case 2 it is in general extremely difficult to obtain the signal enhancement in the $\gamma\gamma$ channel. The scan naturally tends to stay in the regions of parameter space favored by all constraints. It is therefore no surprise that among the points scanned for Case 1 only two presented a $\gamma\gamma$ rate in the range $1.2-2$, thanks to the reduced coupling of the signal Higgs boson to the bottom quarks. Such points present χ^2 contributions to the relic density of order several tens, and the χ^2 contribution to $\mathrm{BR}\,(\mathrm{B_s} \to \mu^+\mu^-)$ is of order 100. In Case 2 we found a dozen such points, for which the contribution to the relic density is even worse.

In Case 3 one could expect to obtain an enhancement of $R_{h_{\rm sig}}(\gamma\gamma)$ by adding the individual rates for both almost degenerate light scalars. However, the posterior pdf in the ($R_{h_1+h_2}(\gamma\gamma)$, $R_{h_1+h_2}(ZZ)$) plane is remarkably similar to the one shown in Fig. 9(a) for Case 1, due to the large singlet component of h_2. In fact, in Case 3 we were not able to find a single point with the enhanced $\gamma\gamma$ rate. Since Case 3 is a subset of Case 2 in terms of the favored parameter space, and the rates in the $\gamma\gamma$ and ZZ channel do not show interesting features, we will not consider it any further.

4.4 Prospects for DM direct detection and $\mathrm{BR}\,(\mathrm{B_s} \to \mu^+\mu^-)$

In this subsection we will discuss the impact of limits from direct DM searches on the allowed parameter space of the CNMSSM. This kind of experiments is complementary to direct LHC SUSY searches, as they are capable of testing neutralino WIMP mass ranges beyond the current and future reach of the LHC, and therefore could add new pieces of information to the global picture.

At present the most stringent limit on the spin-independent cross section $\sigma_p^{\rm SI}$ comes from XENON100 [77]. In supersymmetric models it can then be plotted as a function of the neutralino mass in the form of an exclusion limit in the (m_χ, $\sigma_p^{\rm SI}$) plane. In this study, we did not include the upper bound on $\sigma_p^{\rm SI}$ from XENON100 in the likelihood function, since it was shown in [41] that, given the large theoretical uncertainties (of order 5 to 10), it typically does not affect the shape of the posterior pdf.

In Fig. 10(a), we present the posterior pdf in the (m_χ, $\sigma_p^{\rm SI}$) plane for the Case 1. The solid red line shows the most recent 90% CL upper exclusion limit by the XENON100 Collaboration. One can see that the two high posterior probability regions (from SC on the left and AF on the right) are located well below it. A small 95% credible region (corresponding to the FP/HB region with the lightest neutralino being a mixture of bino and higgsino) is almost (but not yet entirely) excluded, even taking into account significant theoretical uncertainties. One can also notice that XENON1T, a future ton-size DM detector (projected sensitivity represented as the dashed gray line), will be in a position to test the 68% credible regions.

The impact of the XENON100 limit in Case 2 is even stronger. In Fig. 10(b) we show the posterior in the (m_χ, $\sigma_p^{\rm SI}$) plane. The high probability region above the experimental line presents the features of the FP/HB region: $\mu_{\rm eff} \sim 200\,\mathrm{GeV}$, and the lightest neutralino is a mixture of bino and higgsino. As a consequence, the spin-independent neutralino-proton cross section tends to be larger, so that the region has the potential of being ruled out soon. Since we force $m_{h_2} \sim 126\,\mathrm{GeV}$, the favored region of m_χ is pushed down to $\lesssim 240\,\mathrm{GeV}$. This is important as it implies that a significant fraction of the parameter space for the case in which the role of the SM-like Higgs is

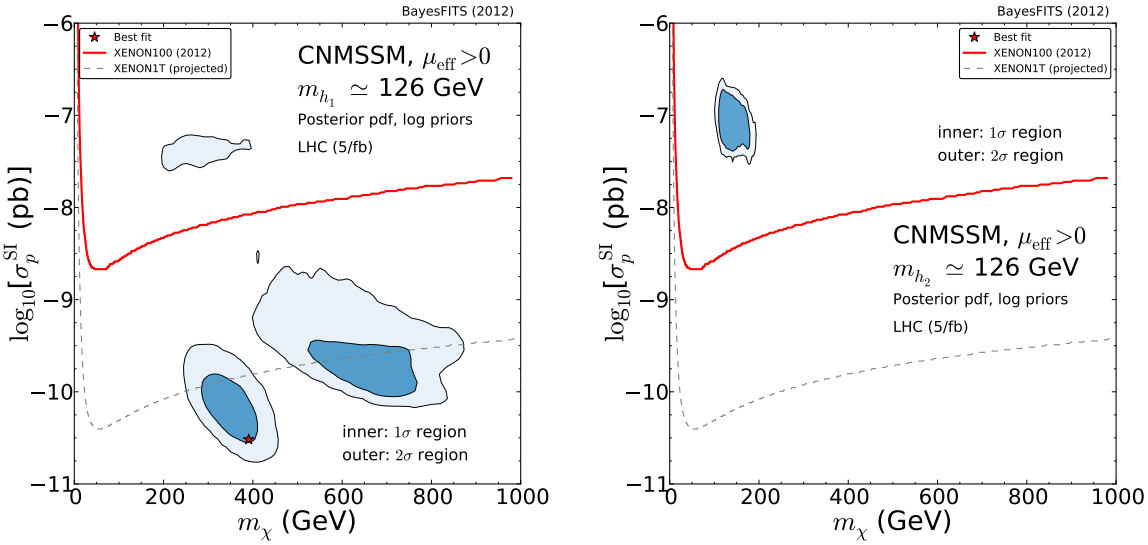

(a) (b)

Figure 10: Marginalized 2D posterior pdf in the (m_χ, $\sigma_p^{\rm SI}$) plane of the CNMSSM constrained by the experiments listed in Table 1 in (a) Case 1 and (b) Case 2. The solid red line shows the 90% CL exclusion bound by XENON100 (not included in the likelihood), and the dashed gray line the projected sensitivity for XENON1T. The color code is the same as in Fig. 2.

played by the second-to-the-lightest CP-even scalar is strongly disfavored.

Notice that the SC region is not shown in Fig. 10(b) since the neutralino is a nearly pure singlino there, so that $\sigma_p^{\rm SI}$ is several orders of magnitude below the XENON100 bound (and below the range shown in the figure). However, we would like to point out that in Case 2 (and Case 3) strong constraints on the full parameter space can be placed as a result of the interplay between the limits provided by two completely different experiments – that test different observables by means of different experimental techniques – namely LHCb and XENON100. This is illustrated in Figs. 11(a) and 11(b), where we show the posterior pdf in the $\left({\rm BR}\left({\rm B_s}\to\mu^+\mu^-\right), \sigma_{\rm p}^{\rm SI}\right)$ plane for Case 1 and Case 2, respectively. The solid blue horizontal line shows the minimum 90% CL upper bound on $\sigma_p^{\rm SI}$ by XENON100 (obtained at $m_\chi \sim 50\,{\rm GeV}$), and the dotted blue horizontal line the corresponding projected sensitivity for XENON1T. The pink vertical band encompasses the 1σ experimental uncertainty on the recent LHCb measurement of ${\rm BR}\left({\rm B_s}\to\mu^+\mu^-\right)$ [35]. Figure 11(b) shows that, for Cases 2 and 3, in the SC region ${\rm BR}\left({\rm B_s}\to\mu^+\mu^-\right)$ is strongly enhanced, due to the large values assumed by $\tan\beta$ there, and it could be excluded by the next updated results from LHCb.

4.5 Fine-tuning

In this subsection we will address the issue of fine-tuning. Note that we will not delve into it, nor will we discuss which values of fine-tuning are acceptable or not from the point of view of naturalness. Our aim here is to simply present an estimate of fine-tuning (provided as an output by NMSSMTools v3.2.1) for the allowed parameter space of the model, leaving aside the discussion of the viability of the model itself, which would be a matter of personal prejudices.

The mass of the Z boson (which determines the EW symmetry breaking scale) can be expressed

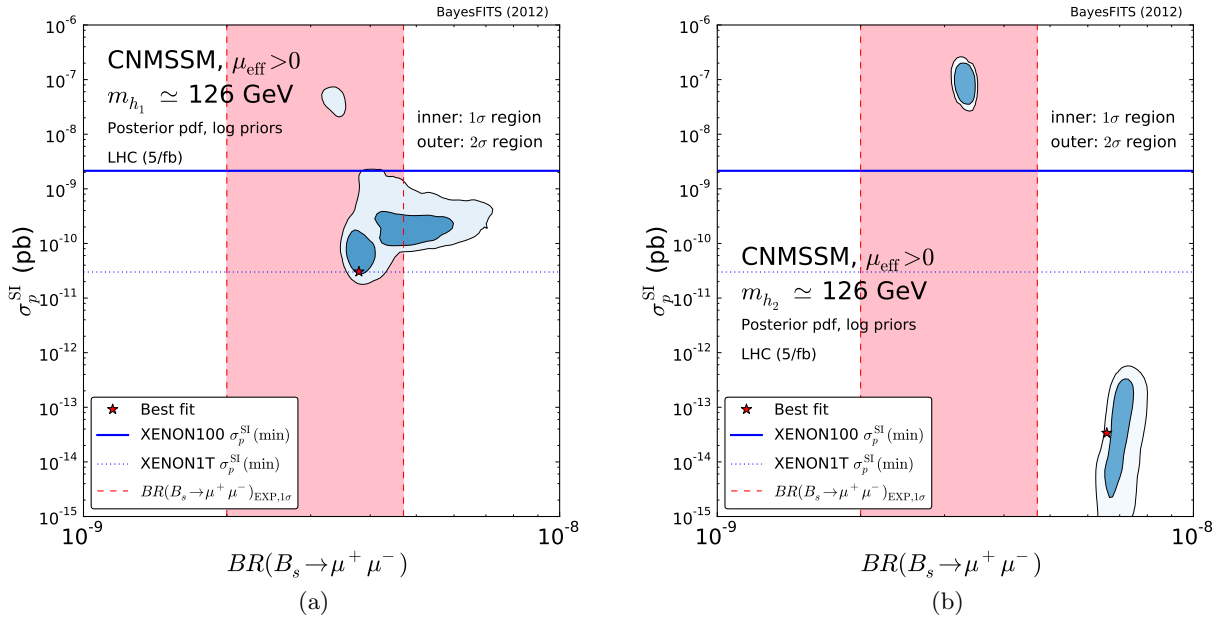

Figure 11: Marginalized 2D posterior pdf in the (BR (B$_{\rm s}\to\mu^+\mu^-$), $\sigma_p^{\rm SI}$) plane of the CNMSSM constrained by the experiments listed in Table 1 in (a) Case 1 and (b) Case 2. The color code is the same as in Fig. 2. The solid blue horizontal line shows the minimum 90% CL upper bound on $\sigma_p^{\rm SI}$ by XENON100 (not included in the likelihood), and the dotted blue horizontal line the corresponding projected sensitivity for XENON1T. The pink vertical band shows the 1σ experimental uncertainty on the recent measurement of BR (B$_{\rm s}\to\mu^+\mu^-$) [35] (which is included in the likelihood).

in terms of the supersymmetric parameters through the minimization condition of the Higgs potential,

$$\frac{M_Z^2}{2} = -\mu^2 + \frac{m_{H_d}^2 - m_{H_u}^2 \tan^2\beta}{(\tan^2\beta - 1)}. \tag{18}$$

The fine-tuning problem of the MSSM [78] amounts to the fact that the parameters m_{H_u}, m_{H_d} and μ need to be simultaneously tuned to a high precision to reproduce the correct value of M_Z. In the NMSSM μ is replaced by $\mu_{\rm eff}$.

In the framework of the unified theory, at the GUT scale $m_{H_u} = m_{H_d} = m_0$. They are then evolved down to the EW scale by means of the RGE's. Therefore, the right-hand side of Eq. (18) depends on the parameters of the model at the GUT scale.

The measure of fine-tuning associated with the parameter p_i of the model is defined as [79, 78]

$$\Delta_{p_i} = \left| \frac{\partial \log M_Z^2}{\partial \log p_i^2} \right|. \tag{19}$$

In the CNMSSM, $p_i = \{m_0, m_{1/2}, A_0, \lambda, \kappa\}$. We do not present the fine-tuning measure due to the top-quark Yukawa coupling, following the approach adopted in [73], and quantifying the fine-tuning associated only with the supersymmetric parameters. We define the fine-tuning measure Δ for a given model point as the maximal contribution to fine-tuning among all the model's parameters for that point,

$$\Delta = {\rm Max}(\Delta_{p_i}). \tag{20}$$

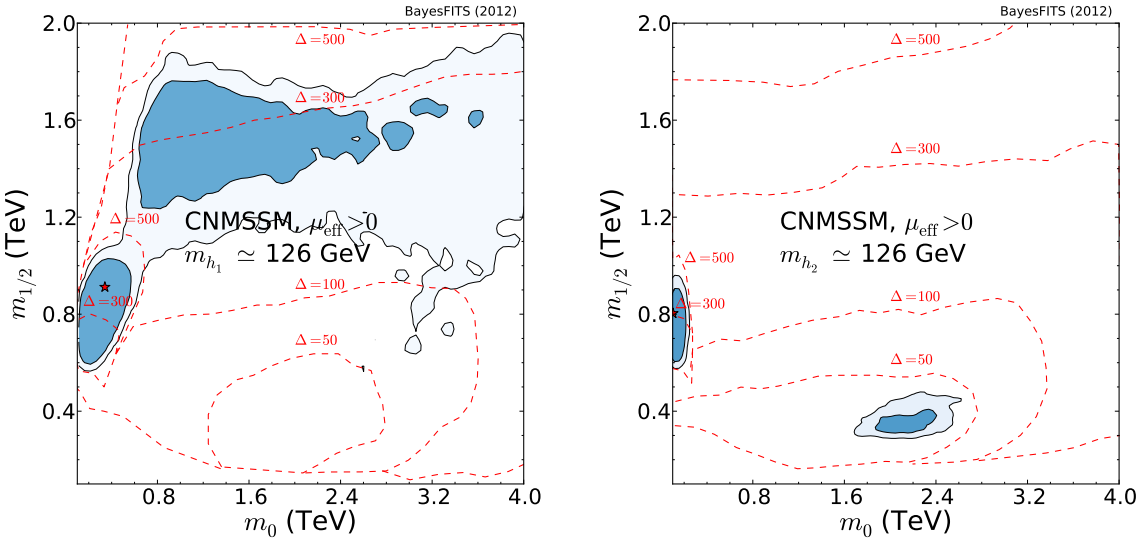

Figure 12: Iso-contours of the fine-tuning measure Δ (dashed red lines) superimposed to the 2D posterior pdf for (a) Case 1 and (b) Case 2. The color code is the same as in Fig. 2.

In Figs. 12(a) and 12(b) we present the iso-contours of the fine-tuning measure Δ in the (m_0, $m_{1/2}$) plane for Cases 1 and 2, respectively. The iso-contours reflect the value of Δ for the vast majority of the points included. They are superimposed on the 2D posterior distributions. Case 1 presents very CMSSM-like behaviour, where smaller fine-tuning can be achieved only in the FP/HB region due to the relatively low values of $\mu_{\rm eff}$. Note that for the same reason Δ is larger in the SC region which is characterized by larger $\mu_{\rm eff}$. On the other hand, Case 2 is less fine-tuned ($\Delta < 50$ in a vast region of the parameter space allowed at 2σ), which is a reflection of the fact that the parameter space is already highly constrained by the requirement of $m_{h_2} \sim 126$ GeV. In Figs. 13(a) and 13(b) we show for what percentage of the total number of allowed points each of the p_i's yields maximal fine-tuning. For example, κ gives maximal fine-tuning for 94% of the points in Case 1,

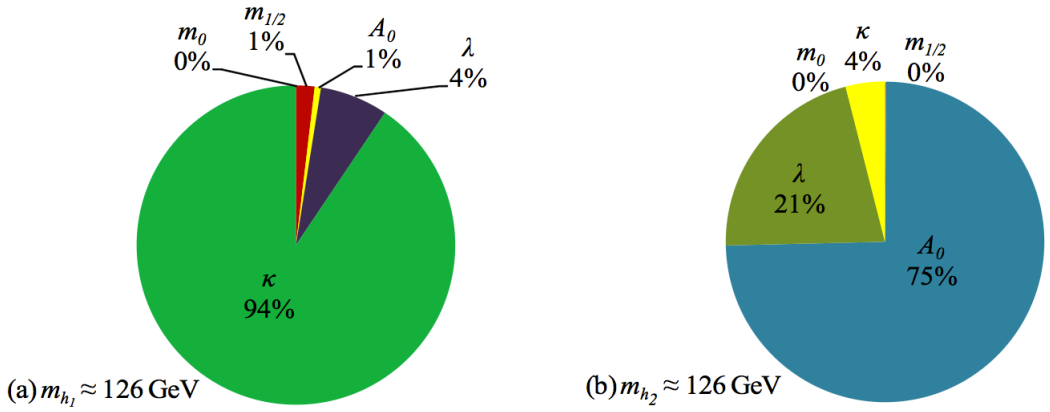

Figure 13: Pie-charts showing the fraction of the total number of allowed points that yields maximum fine-tuning by each of the p_i's for (a) Case 1 and (b) Case 2.

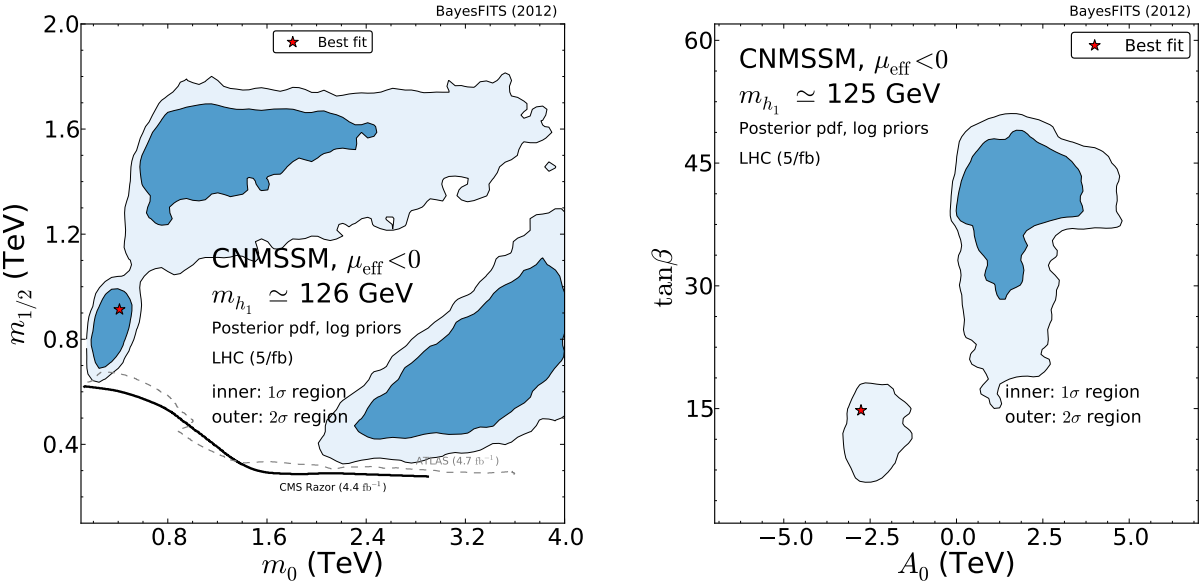

(a) (b)

Figure 14: Marginalized 2D posterior pdf in (a) the (m_0, $m_{1/2}$) plane and (b) the (A_0, $\tan\beta$) plane of the CNMSSM constrained by the experiments listed in Table 1, for Case 1 without $(g-2)_\mu$ and with $\mu_{\rm eff} < 0$. The color code is the same as in Fig. 2.

while A_0 is the main contributor for the vast majority of the points in Case 2.

4.6 Relaxing $(g-2)_\mu$ and the case of negative $\mu_{\rm eff}$

In our recent study of the CMSSM [29] we considered the effect of relaxing the $\delta\,(g-2)_\mu$ constraint. The reason was based on the observation that the poor fit of the CMSSM was the result of basically that single constraint, which simply could not be reproduced after including especially direct superpartner mass limits from the LHC. This appears to be a general feature of all SUSY models where slepton and squark masses are assumed to be comparable, including simple unified models like the CMSSM or CNMSSM. We simply state it as a conclusion reached by many studies. While we do not feel to be in a position to comment on the reliability of theoretical calculations of the SM $(g-2)_\mu$ which are strongly affected by non-perturbative effects related to low-energy strong interactions, especially the hadronic light-by-light contribution (for more details see, e.g., the Introduction of [29] and references therein), we believe that it thus makes sense to consider global scans where the constraint is removed. We showed in [29] that for the CMSSM the better fit was obtained with $\mu < 0$ thanks to the constraints from b-physics, which present a much better χ^2 for this choice of parameters.

Relaxing the $(g-2)_\mu$ constraint in the CNMSSM while keeping $\mu_{\rm eff}$ positive has no apparent impact on the posterior distributions both for the parameters of the model as for the measured observables. Such a behavior was to be expected and has already been observed in [29]. We also confirm that the better overall fit is obtained with $\mu_{\rm eff} < 0$ for basically the same reasons as in the CMSSM.

In Fig. 14(a) we show the 2D posterior pdf in the (m_0, $m_{1/2}$) plane for Case 1, where we ignored the constraint from $\delta\,(g-2)_\mu$ and set $\mathrm{sgn}(\mu_{\rm eff}) = -1$. Differently from the CMSSM, where

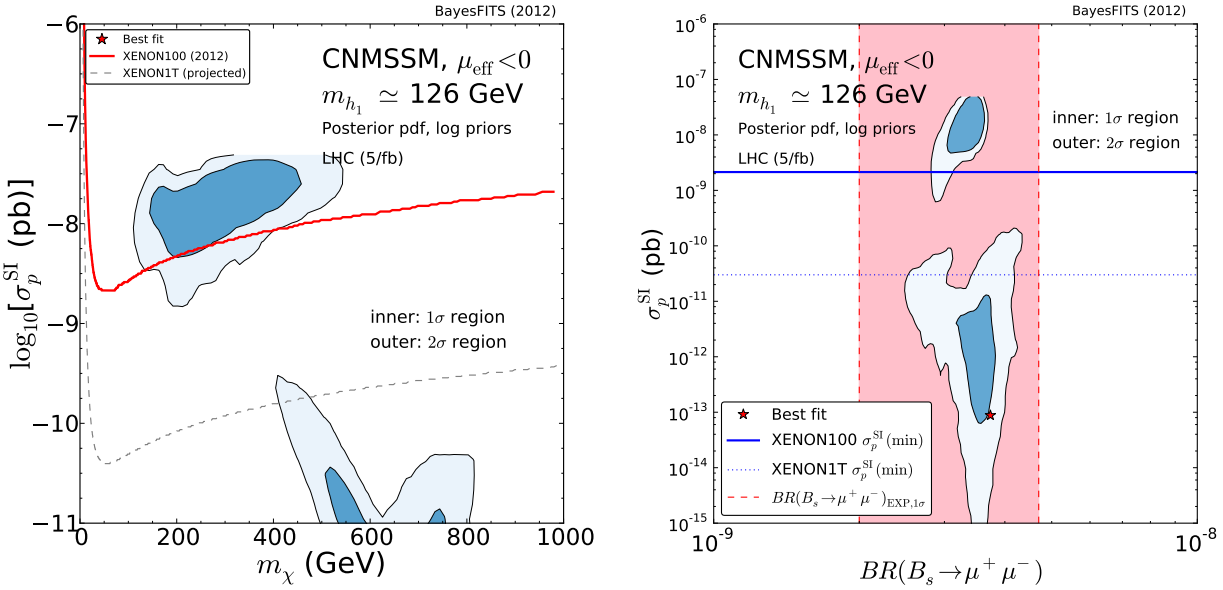

Figure 15: Marginalized 2D posterior pdf in (a) the (m_χ, $\sigma_p^{\rm SI}$) plane and (b) the (BR ($\rm B_s \to \mu^+\mu^-$), $\sigma_p^{\rm SI}$) plane of the CNMSSM constrained by the experiments listed in Table 1, for Case 1 without $(g-2)_\mu$ and with $\mu_{\rm eff} < 0$. The color code is the same as in Figs. 10 and 11.

one could observed a clear predominance of the AF region, in the CNMSSM the SC, AF and FP/HB regions of parameter space now seem to be equally probable. This is not likely to be an intrinsic difference between the CMSSM and the CNMSSM; it is more probably due to the fact that the constraints are implemented with different numerical tools in the two models, as explained exhaustively at the beginning of Sec. 4. We note here that the global likelihood becomes flat over the regions of parameter space allowed by the relic density, and very little information can be extracted from the posterior.

In Fig. 14(b) we show the same posterior pdf in the (A_0, $\tan\beta$) plane for Case 1. As was the case for the CMSSM, one can see that the distribution of $\tan\beta$ tends to favor slightly smaller values than in the positive $\mu_{\rm eff}$ case, particularly in the AF region.

In Fig. 15(a) we show the 2D posterior pdf in the (m_χ, $\sigma_p^{\rm SI}$) plane for Case 1. Since the posterior in the FP/HB region is much more extended with respect to the positive $\mu_{\rm eff}$ case, a large region of parameter space lies above the XENON100 bound, and has the potential of being tested with modest improvements in sensitivity. On the other hand, as was the case for the CMSSM, the AF region ($m_\chi > 400\,$GeV and $\sigma_p^{\rm SI} < 10^{-10}\,$pb) is not likely to be further constrained by the new spin-independent cross section measurements planned for the next years, including XENON1T.

We shall analyze the χ^2 contributions from the individual constraints in the next subsection. Here we only repeat that, when the $(g-2)_\mu$ constraint is relaxed, the better χ^2 can be obtained for $\mu_{\rm eff} < 0$ thanks to the improved fit to BR ($\rm B_s \to \mu^+\mu^-$) and BR $\left(\overline{\rm B} \to {\rm X_s}\gamma\right)$. To illustrate this feature we show in Fig. 15(b) the 2D posterior pdf in the (BR ($\rm B_s \to \mu^+\mu^-$), $\sigma_p^{\rm SI}$) plane for Case 1. When $\mu_{\rm eff} < 0$, BR ($\rm B_s \to \mu^+\mu^-$) receives negative SUSY contributions that improve the fit over all parameter space, and particularly in the AF region, where the calculated values are pushed below the SM value.

4.7 Mass spectrum and the best-fit points

In Figs. 16(a) and 16(b), we show the 1D marginalized posterior pdf's for the SUSY mass spectrum in Case 1 and Case 2, respectively. The narrow lines indicate the 95% credibility regions, and the thick bars the 68% credibility regions.

Figure 16(a) shows the CMSSM-like character of Case 1, since h_3, a_2 and χ_5 are all heavy and effectively decoupled from the low scale spectrum. For Case 2, Fig. 16(b) shows that requiring $m_{h_2} \sim 126\,\text{GeV}$ forces the particles of the Higgs sector to be quite light, while the sfermions remain heavy, although they tend to be lighter than in Case 1, since m_{h_1} is lighter and it requires smaller loop corrections. The latter affect the scale of the stop and, through the assumption of unification, the other sfermions.

In Fig. 16(c) we show the mass spectrum for Case 1 where we neglect $\delta\,(g-2)_\mu$ and set $\mu_{\text{eff}} < 0$.

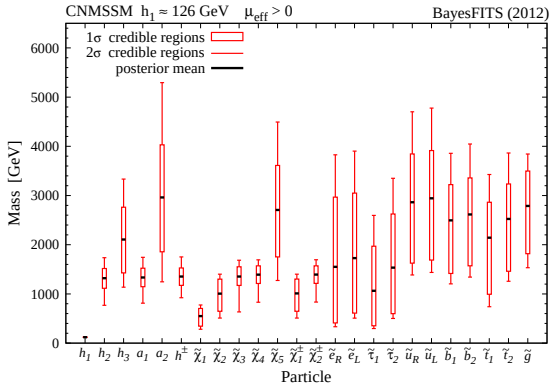

(a)

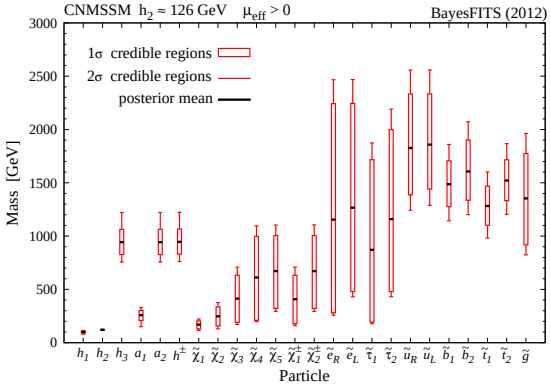

(b)

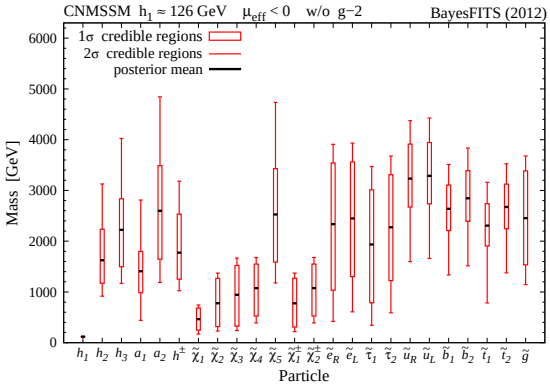

(c)

Figure 16: SUSY mass spectra of the CNMSSM with $\mu_{\text{eff}} > 0$ for (a) Case 1 and (b) Case 2. (c) SUSY spectrum with $\mu_{\text{eff}} < 0$ and no $(g-2)_\mu$ in Case 1. The narrow lines indicate the 95% credibility ranges and the thick bars the 68% credibility regions.

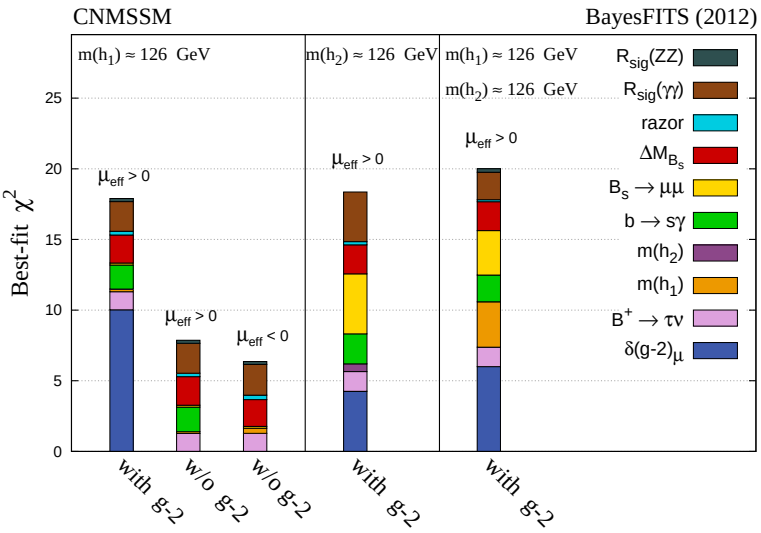

Figure 17: Individual χ^2 contributions to the best-fit points of the scans considered.

Again we confirm the CMSSM-like nature.

In Fig. 17 we show the individual χ^2 contributions of the applied constraints to the best-fit point, for the cases considered in this study. As could be expected, in Case 1 the main contribution comes from $\delta\left(g-2\right)_\mu$, once more confirming the CMSSM-like character of this scenario. In Case 2 the contribution from $\delta\left(g-2\right)_\mu$ is comparable to the one from $\mathrm{BR}\left(\mathrm{B_s} \to \mu^+\mu^-\right)$, due to the singlino character of neutralino which favors higher $\tan\beta$, as explained in Sec. 4.4. When $\mu_{\mathrm{eff}} > 0$, relaxing the $(g-2)_\mu$ constraint does not change significantly the contributions to χ^2_{min} due to the other constraints. This shows that the χ^2 due to $(g-2)_\mu$ is fairly homogeneous throughout the parameter space not yet excluded by direct LHC SUSY searches. However, for negative μ_{eff} the total χ^2 improves by around 1-2 units, thanks to the improved fit to $\mathrm{BR}\left(\overline{\mathrm{B}} \to \mathrm{X_s}\gamma\right)$, for which the contribution from the chargino-stop loop changes sign and tends to enhance the branching ratio, towards the experimental value [80]. As a consequence, the overall fit to the experimental measurement improves.

One can finally notice that the contributions to χ^2_{min} due to $R_{h_{\mathrm{sig}}}(\gamma\gamma)$ are sizeable in all three cases, as was explained in Sec. 4.3.

In Table 3 we show the parameters of the best-fit points obtained in our scans.

5 Summary and conclusions

In this paper we have presented the first global analysis of the CNMSSM which included the measurement of the mass and decay cross sections of the Higgs-like resonance observed at the LHC, the first evidence of nonzero $\mathrm{BR}\left(\mathrm{B_s} \to \mu^+\mu^-\right)$ at LHCb, SUSY mass limits from direct searches, as well as the updated value of the top mass. We discussed in detail the possibility of either one of the lightest CP-even Higgs bosons of the model playing the role of the SM-like Higgs (Case 1 and Case 2 in the text) and that of the observed excess being due to a combination of two of them,

	m_0	$m_{1/2}$	A_0	$\tan\beta$	λ	$m_{h_{\rm sig}}$	Δ	χ^2_{min}
With $(g-2)_\mu$								
Case 1, $\mu_{\rm eff} > 0$	340.9	911.9	-2546	12.0	0.017	124.5	427	17.91
Case 2, $\mu_{\rm eff} > 0$	102.8	803.6	-295.0	32.1	0.006	123.5	396	18.45
Case 3, $\mu_{\rm eff} > 0$	124.7	958.8	-356.7	33.7	0.001	120.3, 126.2	480	20.08
No $(g-2)_\mu$								
Case 1, $\mu_{\rm eff} < 0$	410.2	913.3	-2764	14.8	0.017	123.9	455	6.40

Table 3: CNMSSM input parameters, Higgs masses and fine-tuning measure for the best-fit points of our scans. Masses and A_0 are in GeV.

both lying within the range $\sim 123 - 129\,\text{GeV}$, after inclusion of a 3-GeV theoretical error on the Higgs mass calculation (Case 3 in the text).

Contrary to what is generally believed, we found that the CNMSSM does allow a SM-like h_1 as heavy as 125 GeV, especially in the stau coannihilation region where the scan obtains a good compromise between the relic density and the h_1 mass constraint owing to large negative A_0 values. The calculated value of m_{h_1} is larger than what was observed for the CMSSM in the same region thanks to the increased value of the top pole mass. The overall fit is somewhat spoiled by the requirement of having $R_{h_1}(\gamma\gamma)$ consistent with the value reported by the CMS collaboration, since it is virtually impossible to obtain an enhancement in the cross section rate in Case 1. A similar conclusion can be drawn for Case 2 where, in turn, h_2 is required to have a mass around 126 GeV, which can also be achieved but at the cost of a poor fit to other observables. Case 3, with almost degenerate h_1 and h_2 was found not to be as interesting as anticipated, since the combined $R_{h_1+h_2}(\gamma\gamma)$ almost never exceeds 1, besides the fact that the high credibility posterior regions mimic those of Case 2.

We also provided estimates of fine-tuning due to the various input parameters of the model in the form of iso-contours in the (m_0, $m_{1/2}$) plane for Cases 1 and 2. We noted that the maximum fine-tuning for most of the parameter space comes from two different sources in the two cases.

Finally, we assessed the effects of abandoning the $(g-2)_\mu$ constraint since it cannot be reproduced in the CNMSSM, and more generally SUSY models with slepton-squark unification. In this case the overall fit actually improves considerably for $\mu_{\rm eff} < 0$, due to a better agreement of the model's predictions for b-physics observables with experimental data, similarly to the CMSSM.

ACKNOWLEDGMENTS

S.M. would like to thank Cyril Hugonie for useful e-mail exchange regarding model implementation in NMSSMTools. L.R. thanks Gino Isidori and Matteo Palutan for helpful comments about $\text{BR}\,(\text{B}_\text{s} \to \mu^+\mu^-)$.

This work has been funded in part by the Welcome Programme of the Foundation for Polish Science. K.K. is supported by the EU and MSHE grant N POIG.02.03.00-00-013/09. L.R. is also supported in part by the Polish National Science Centre grant N N202 167440, an STFC consortium grant of Lancaster, Manchester and Sheffield Universities and by the EC 6th Framework Programme MRTN-CT-2006-035505. The use of the CIS computer cluster at NCBJ is gratefully acknowledged.

References

[1] **CMS Collaboration** Collaboration, S. Chatrchyan *et al.*, "Observation of a new boson at a mass of 125 GeV with the CMS experiment at the LHC," *Phys.Lett.* **B716** (2012) 30–61, arXiv:1207.7235 [hep-ex].

[2] **ATLAS Collaboration** Collaboration, G. Aad *et al.*, "Observation of a new particle in the search for the Standard Model Higgs boson with the ATLAS detector at the LHC," *Phys.Lett.* **B716** (2012) 1–29, arXiv:1207.7214 [hep-ex].

[3] "Combination of standard model higgs boson searches and measurements of the properties of the new boson with a mass near 125 gev," Tech. Rep. CMS-PAS-HIG-12-045, CERN, Geneva, 2012

[4] "Updated results on the new boson discovered in the search for the standard model higgs boson in the zz to 4 leptons channel in pp collisions at sqrt(s)=7 and 8 tev," Tech. Rep. CMS-PAS-HIG-12-041, CERN, Geneva, 2012

[5] "Updated atlas results on the signal strength of the higgs-like boson for decays into ww and heavy fermion final states," Tech. Rep. ATLAS-CONF-2012-162, CERN, Geneva, Nov, 2012

[6] J. E. Kim and H. P. Nilles, "The mu Problem and the Strong CP Problem," *Phys. Lett. B* **138** (1984) 150.

[7] U. Ellwanger, C. Hugonie, and A. M. Teixeira, "The Next-to-Minimal Supersymmetric Standard Model," *Phys.Rept.* **496** (2010) 1–77, arXiv:0910.1785 [hep-ph].

[8] M. Maniatis, "The Next-to-Minimal Supersymmetric extension of the Standard Model reviewed," *Int.J.Mod.Phys.* **A25** (2010) 3505–3602, arXiv:0906.0777 [hep-ph].

[9] S. King, M. Muhlleitner, and R. Nevzorov, "NMSSM Higgs Benchmarks Near 125 GeV," *Nucl.Phys.* **B860** (2012) 207–244, arXiv:1201.2671 [hep-ph]. ; J. Cao *et al.*, "A SM-like Higgs near 125 GeV in low energy SUSY: a comparative study for MSSM and NMSSM," *JHEP* **1203** (2012) 086, arXiv:1202.5821 [hep-ph]. ; D. A. Vasquez *et al.*, "The 125 GeV Higgs in the NMSSM in light of LHC results and astrophysics constraints," arXiv:1203.3446 [hep-ph]. ; J. Rathsman and T. Rossler, "Closing the Window on Light Charged Higgs Bosons in the NMSSM," arXiv:1206.1470 [hep-ph]. ; D. Das, U. Ellwanger, and P. Mitropoulos, "A 130 GeV photon line from dark matter annihilation in the NMSSM," *JCAP* **1208** (2012) 003, arXiv:1206.2639 [hep-ph].

[10] J. F. Gunion, Y. Jiang, and S. Kraml, "Could two NMSSM Higgs bosons be present near 125 GeV?," *Phys.Rev.* **D86** (2012) 071702, arXiv:1207.1545 [hep-ph]. ; J. F. Gunion, Y. Jiang, and S. Kraml, "Diagnosing Degenerate Higgs Bosons at 125 GeV," arXiv:1208.1817 [hep-ph].

[11] R. Benbrik, M. Gomez Bock, S. Heinemeyer, O. Stal, G. Weiglein, *et al.*, "Confronting the MSSM and the NMSSM with the Discovery of a Signal in the two Photon Channel at the LHC," *Eur.Phys.J.* **C72** (2012) 2171, arXiv:1207.1096 [hep-ph]. ; K. J. Bae, K. Choi, E. J. Chun, S. H. Im, C. B. Park, *et al.*, "Peccei-Quinn NMSSM in the light of 125 GeV Higgs," *JHEP* **1211** (2012) 118, arXiv:1208.2555 [hep-ph]. ; Z. Kang, T. Li, J. Li, and Y. Liu, "A Rediatively Light Stop Saves the Best Global Fit for Higgs Boson Mass and Decays," arXiv:1208.2673

[hep-ph]. ; T. Cheng, J. Li, T. Li, X. Wan, Y. K. Wang, *et al.*, "Toward the Natural and Realistic NMSSM with and without R-Parity," arXiv:1207.6392 [hep-ph]. ; M. Perelstein and B. Shakya, "XENON100 Implications for Naturalness in the MSSM, NMSSM and lambda-SUSY," arXiv:1208.0833 [hep-ph]. ; G. Belanger, U. Ellwanger, J. Gunion, Y. Jiang, and S. Kraml, "Two Higgs Bosons at the Tevatron and the LHC?," arXiv:1208.4952 [hep-ph].

[12] J. Cao, Z. Heng, J. M. Yang, and J. Zhu, "Status of low energy SUSY models confronted with the LHC 125 GeV Higgs data," *JHEP* **1210** (2012) 079, arXiv:1207.3698 [hep-ph].

[13] G. Chalons and F. Domingo, "Analysis of the Higgs potentials for two doublets and a singlet," arXiv:1209.6235 [hep-ph]. ; G. Belanger, U. Ellwanger, J. F. Gunion, Y. Jiang, S. Kraml, *et al.*, "Higgs Bosons at 98 and 125 GeV at LEP and the LHC," arXiv:1210.1976 [hep-ph]. ; I. Gogoladze, B. He, and Q. Shafi, "Inverse Seesaw in NMSSM and 126 GeV Higgs Boson," arXiv:1209.5984 [hep-ph]. ; D. E. Lopez-Fogliani, "Light Higgs and neutralino dark matter in the NMSSM," *J.Phys.Conf.Ser.* **384** (2012) 012014.

[14] U. Ellwanger, "A Higgs boson near 125 GeV with enhanced di-photon signal in the NMSSM," *JHEP* **1203** (2012) 044, arXiv:1112.3548 [hep-ph].

[15] U. Ellwanger and C. Hugonie, "Higgs bosons near 125 GeV in the NMSSM with constraints at the GUT scale," *Adv.High Energy Phys.* **2012** (2012) 625389, arXiv:1203.5048 [hep-ph].

[16] M. Bastero-Gil, C. Hugonie, S. King, D. Roy, and S. Vempati, "Does LEP prefer the NMSSM?," *Phys.Lett.* **B489** (2000) 359–366, arXiv:hep-ph/0006198 [hep-ph].

[17] A. Delgado, C. Kolda, J. P. Olson, and A. de la Puente, "Solving the Little Hierarchy Problem with a Singlet and Explicit μ Terms," *Phys.Rev.Lett.* **105** (2010) 091802, arXiv:1005.1282 [hep-ph].

[18] U. Ellwanger, G. Espitalier-Noel, and C. Hugonie, "Naturalness and Fine Tuning in the NMSSM: Implications of Early LHC Results," *JHEP* **1109** (2011) 105, arXiv:1107.2472 [hep-ph].

[19] G. G. Ross and K. Schmidt-Hoberg, "The Fine-Tuning of the Generalised NMSSM," *Nucl.Phys.* **B862** (2012) 710–719, arXiv:1108.1284 [hep-ph].

[20] U. Ellwanger, "Enhanced di-photon Higgs signal in the Next-to-Minimal Supersymmetric Standard Model," *Phys.Lett.* **B698** (2011) 293–296, arXiv:1012.1201 [hep-ph].

[21] J. F. Gunion, H. E. Haber, and T. Moroi, "Will at least one of the Higgs bosons of the next-to-minimal supersymmetric extension of the standard model be observable at LEP-2 or the LHC?," *eConf* **C960625** (1996) LTH095, arXiv:hep-ph/9610337 [hep-ph]

[22] G. L. Kane, C. F. Kolda, L. Roszkowski, and J. D. Wells, "Study of constrained minimal supersymmetry," *Phys. Rev.* **D49** (1994) 6173–6210, arXiv:hep-ph/9312272 [hep-ph].

[23] J. Ellis, J. F. Gunion, H. E. Haber, L. Roszkowski, and F. Zwirner, "Higgs bosons in a nonminimal supersymmetric model," *Phys. Rev. D* **39** (Feb, 1989) 844–869. http://link.aps.org/doi/10.1103/PhysRevD.39.844

[24] A. Djouadi, U. Ellwanger, and A. Teixeira, "The Constrained next-to-minimal supersymmetric standard model," *Phys.Rev.Lett.* **101** (2008) 101802, arXiv:0803.0253 [hep-ph]

[25] A. Djouadi, U. Ellwanger, and A. Teixeira, "Phenomenology of the constrained NMSSM," *JHEP* **0904** (2009) 031, arXiv:0811.2699 [hep-ph].

[26] S. Heinemeyer, W. Hollik, and G. Weiglein, "FeynHiggs: A Program for the calculation of the masses of the neutral CP even Higgs bosons in the MSSM," *Comput.Phys.Commun.* **124** (2000) 76–89, arXiv:hep-ph/9812320 [hep-ph].

[27] B. Allanach, "SOFTSUSY: a program for calculating supersymmetric spectra," *Comput.Phys.Commun.* **143** (2002) 305–331, arXiv:hep-ph/0104145 [hep-ph].

[28] S. Heinemeyer, O. Stal, and G. Weiglein, "Interpreting the LHC Higgs Search Results in the MSSM," *Phys.Lett.* **B710** (2012) 201–206, arXiv:1112.3026 [hep-ph].

[29] A. Fowlie, M. Kazana, K. Kowalska, S. Munir, L. Roszkowski, *et al.*, "The CMSSM Favoring New Territories: The Impact of New LHC Limits and a 125 GeV Higgs," *Phys.Rev.* **D86** (2012) 075010, arXiv:1206.0264 [hep-ph].

[30] J. F. Gunion, Y. Jiang, and S. Kraml, "The Constrained NMSSM and Higgs near 125 GeV," *Phys.Lett.* **B710** (2012) 454–459, arXiv:1201.0982 [hep-ph].

[31] D. E. Lopez-Fogliani, L. Roszkowski, R. R. de Austri, and T. A. Varley, "A Bayesian Analysis of the Constrained NMSSM," *Phys.Rev.* **D80** (2009) 095013, arXiv:0906.4911 [hep-ph].

[32] J. F. Gunion, D. E. Lopez-Fogliani, L. Roszkowski, R. Ruiz de Austri, and T. A. Varley, "Next-to-Minimal Supersymmetric Model Higgs Scenarios for Partially Universal GUT Scale Boundary Conditions," *Phys.Rev.* **D84** (2011) 055026, arXiv:1105.1195 [hep-ph].

[33] D. J. MacKay, *Information theory, infernce, and learning algorithms*, Cambridge University Press, Cambridge U.K. (2003).

[34] J. Skilling, *Nested Sampling, in Proceedings of the 24th International Workshop on Bayesian Inference and Maximum Entropy Methods in Science and Engineering*, Garching, Germany, July 2004.

[35] **LHCb Collaboration** Collaboration, R. Aaij *et al.*, "First evidence for the decay $\mathrm{BR}(\mathrm{B_s} \to \mu^+\mu^-)$," arXiv:1211.2674 [Unknown].

[36] K. De Bruyn, R. Fleischer, R. Knegjens, P. Koppenburg, M. Merk, *et al.*, "Probing New Physics via the $B_s^0 \to \mu^+\mu^-$ Effective Lifetime," *Phys.Rev.Lett.* **109** (2012) 041801, arXiv:1204.1737 [hep-ph].

[37] A. J. Buras, J. Girrbach, D. Guadagnoli, and G. Isidori, "On the Standard Model prediction for BR(Bs,d to mu+ mu-)," *Eur.Phys.J.* **C72** (2012) 2172, arXiv:1208.0934 [hep-ph].

[38] **Particle Data Group** Collaboration, J. Beringer *et al.*, "Review of Particle Physics (RPP)," *Phys.Rev.* **D86** (2012) 010001.

[39] C. Hugonie, G. Belanger, and A. Pukhov, "Dark matter in the constrained NMSSM," *JCAP* **0711** (2007) 009, arXiv:0707.0628 [hep-ph].

[40] A. Fowlie *et al.*, "Bayesian Implications of Current LHC and XENON100 Search Limits for the Constrained MSSM," *Phys.Rev.* **D85** (2012) 075012, arXiv:1111.6098 [hep-ph].

[41] L. Roszkowski, E. M. Sessolo, and Y.-L. S. Tsai, "Bayesian Implications of Current LHC Supersymmetry and Dark Matter Detection Searches for the Constrained MSSM," *Phys.Rev.* **D86** (2012) 095005, arXiv:1202.1503 [hep-ph].

[42] "Search for supersymmetry with the razor variables at CMS," Tech. Rep. CMS-PAS-SUS-12-005, CERN, Geneva, 2012

[43] https://twiki.cern.ch/twiki/bin/view/CMSPublic/PhysicsResults

[44] **WMAP** Collaboration, E. Komatsu *et al.*, "Seven-Year Wilkinson Microwave Anisotropy Probe (WMAP) Observations: Cosmological Interpretation," *Astrophys. J. Suppl.* **192** (2011) 18, arXiv:1001.4538 [astro-ph.CO]

[45] J. P. Miller, E. de Rafael, and B. L. Roberts, "Muon (g-2): Experiment and theory," *Rept.Prog.Phys.* **70** (2007) 795, arXiv:hep-ph/0703049 [hep-ph].

[46] http://www.slac.stanford.edu/xorg/hfag/rare/2012/radll/index.html

[47] **Heavy Flavor Averaging Group** Collaboration, Y. Amhis *et al.*, "Averages of b-hadron, c-hadron, and tau-lepton properties as of early 2012," arXiv:1207.1158 [hep-ex].

[48] R. R. de Austri, R. Trotta, and L. Roszkowski, "A Markov chain Monte Carlo analysis of the CMSSM," *JHEP* **0605** (2006) 002, arXiv:hep-ph/0602028 [hep-ph].

[49] "Search for the rare decays $B_s \to \mu^+\mu^-$ at the LHC with the ATLAS, CMS and LHCb experiments," Tech. Rep. LHCb-CONF-2012-017, CERN, Geneva, 2012

[50] F. Mahmoudi, S. Neshatpour, and J. Orloff, "Supersymmetric constraints from $B_s \to \mu^+\mu^-$ and $B \to K * \mu^+\mu^-$ observables," *JHEP* **1208** (2012) 092, arXiv:1205.1845 [hep-ph].

[51] **CMS Collaboration** Collaboration, S. Chatrchyan *et al.*, "Inclusive search for squarks and gluinos in pp collisions at sqrt(s) = 7 TeV," *Phys.Rev.* **D85** (2012) 012004, arXiv:1107.1279 [hep-ex]. CMS-SUS-10-009, CERN-PH-EP-2011-099

[52] http:/http://www.th.u-psud.fr/NMHDECAY/nmssmtools.html

[53] M. Bahr, S. Gieseke, M. Gigg, D. Grellscheid, K. Hamilton, *et al.*, "Herwig++ Physics and Manual," *Eur.Phys.J.* **C58** (2008) 639–707, arXiv:0803.0883 [hep-ph].

[54] M. Dobbs and J. B. Hansen, "The HepMC C++ Monte Carlo event record for High Energy Physics," *Comput.Phys.Commun.* **134** (2001) 41–46.

[55] https://cp3.irmp.ucl.ac.be/projects/delphes

[56] B. Allanach, "Impact of CMS Multi-jets and Missing Energy Search on CMSSM Fits," *Phys. Rev.* **D83** (2011) 095019, arXiv:1102.3149 [hep-ph].

[57] P. Bechtle *et al.*, "What if the LHC does not find supersymmetry in the sqrt(s)=7 TeV run?," *Phys.Rev.* **D84** (2011) 011701, arXiv:1102.4693 [hep-ph].

[58] M. Drees, "Supersymmetric Models with Extended Higgs Sector," *Int.J.Mod.Phys.* **A4** (1989) 3635.

[59] A. Djouadi, "The Anatomy of electro-weak symmetry breaking. II. The Higgs bosons in the minimal supersymmetric model," *Phys.Rept.* **459** (2008) 1–241, arXiv:hep-ph/0503173 [hep-ph].

[60] LHC Higgs Cross Section Working Group, S. Dittmaier, C. Mariotti, G. Passarino, and R. Tanaka (Eds.), "Handbook of LHC Higgs Cross Sections: 1. Inclusive Observables," *CERN-2011-002* (CERN, Geneva, 2011) , arXiv:1101.0593 [hep-ph].

[61] LHC Higgs Cross Section Working Group, S. Dittmaier, C. Mariotti, G. Passarino, and R. Tanaka (Eds.), "Handbook of LHC Higgs Cross Sections: 2. Differential Distributions," *CERN-2012-002* (CERN, Geneva, 2012) , arXiv:1201.3084 [hep-ph].

[62] J. Baglio and A. Djouadi, "Higgs production at the lHC," *JHEP* **1103** (2011) 055, arXiv:1012.0530 [hep-ph]

[63] http://cms.web.cern.ch/org/cms-papers-and-results.

[64] F. Feroz, M. Hobson, and M. Bridges, "MultiNest: an efficient and robust Bayesian inference tool for cosmology and particle physics," *Mon.Not.Roy.Astron.Soc.* **398** (2009) 1601–1614, arXiv:0809.3437 [astro-ph].

[65] A. Arbey and F. Mahmoudi, "SuperIso Relic: A program for calculating relic density and flavor physics observables in Supersymmetry," *Comput.Phys.Commun.* **176** (2007) 367–382, arXiv:0906.0369 [hep-ph].

[66] G. Belanger, F. Boudjema, A. Pukhov, and A. Semenov, "micrOMEGAs2.0: a program to calculate the relic density of dark matter in a generic model," *Comput.Phys.Commun.* **181** (2010) 1277–1292, arXiv:hep-ph/0607059 [hep-ph].

[67] M. Spira, "QCD effects in Higgs physics," *Fortsch.Phys.* **46** (1998) 203–284, arXiv:hep-ph/9705337 [hep-ph].

[68] J. R. Ellis, T. Falk, and K. A. Olive, "Neutralino - Stau coannihilation and the cosmological upper limit on the mass of the lightest supersymmetric particle," *Phys.Lett.* **B444** (1998) 367–372, arXiv:hep-ph/9810360 [hep-ph].

[69] T. Nihei, L. Roszkowski, and R. Ruiz de Austri, "Exact cross-sections for the neutralino slepton coannihilation," *JHEP* **0207** (2002) 024, arXiv:hep-ph/0206266 [hep-ph].

[70] J. R. Ellis, K. A. Olive, and Y. Santoso, "Calculations of neutralino stop coannihilation in the CMSSM," *Astropart.Phys.* **18** (2003) 395–432, arXiv:hep-ph/0112113 [hep-ph].

[71] M. Drees and M. M. Nojiri, "The Neutralino relic density in minimal $N = 1$ supergravity," *Phys.Rev.* **D47** (1993) 376–408, arXiv:hep-ph/9207234 [hep-ph].

[72] K. L. Chan, U. Chattopadhyay, and P. Nath, "Naturalness, weak scale supersymmetry and the prospect for the observation of supersymmetry at the Tevatron and at the LHC," *Phys. Rev.* **D58** (1998) 096004, arXiv:hep-ph/9710473.

[73] J. L. Feng, K. T. Matchev, and T. Moroi, "Focus points and naturalness in supersymmetry," *Phys. Rev.* **D61** (2000) 075005, arXiv:hep-ph/9909334.

[74] D. Miller, R. Nevzorov, and P. Zerwas, "The Higgs sector of the next-to-minimal supersymmetric standard model," *Nucl.Phys.* **B681** (2004) 3–30, arXiv:hep-ph/0304049 [hep-ph].

[75] "Search for neutral higgs bosons decaying into tau leptons in the dimuon channel with cms in pp collisions at 7 tev," Tech. Rep. CMS-PAS-HIG-12-007, CERN, Geneva, 2012

[76] F. Mahmoudi, J. Rathsman, O. Stal, and L. Zeune, "Light Higgs bosons in phenomenological NMSSM," *Eur.Phys.J.* **C71** (2011) 1608, arXiv:1012.4490 [hep-ph].

[77] **XENON100 Collaboration** Collaboration, E. Aprile *et al.*, "Dark Matter Results from 225 Live Days of XENON100 Data," *Phys.Rev.Lett.* **109** (2012) 181301, arXiv:1207.5988 [astro-ph.CO].

[78] R. Barbieri and G. Giudice, "Upper Bounds on Supersymmetric Particle Masses," *Nucl.Phys.* **B306** (1988) 63.

[79] J. R. Ellis, K. Enqvist, D. V. Nanopoulos, and F. Zwirner, "Observables in Low-Energy Superstring Models," *Mod.Phys.Lett.* **A1** (1986) 57.

[80] L. Roszkowski, R. Ruiz de Austri, and R. Trotta, "Implications for the Constrained MSSM from a new prediction for $b \to s\gamma$," *JHEP* **0707** (2007) 075, arXiv:0705.2012 [hep-ph].